Master's Thesis of Science

Investigation of ground motion and causes over major urban areas of Bangladesh using time-series SAR interferometry technique

시계열 SAR 간섭 기법을 이용한 방글라데시 주요 도시지역의 지반운동 원인 조사

February 2023

Graduate School of Earth and Environmental Sciences

Seoul National University

BISHWAJIT DHAR

Investigation of ground motion and causes over major urban areas of Bangladesh using time-series SAR interferometry technique

시계열 SAR 간섭 기법을 이용한 방글라데시 주요 도시지역의 지반운동 원인 조사

지도 교수 김 덕 진

이 논문을 이학석사 학위논문으로 제출함

2023 년 2 월

서울대학교 대학원
자연과학대학 지구환경과학부
BISHWAJIT DHAR

BISHWAJIT DHAR 의
이학석사 학위논문을 인준함

2023 년 2 월

Chair	조 양 기	(Seal)
Vice Chair	김 덕 진	(Seal)
Examiner	정 정 교	(Seal)

Abstract

This thesis aims to address the subsidence measurements of major urban areas in Bangladesh. Land subsidence occurs due to drivers of nature (rising water, sediment compaction, tectonics, and reduced sediment supply) or anthropogenic (Fluid extraction). These phenomena are affecting cities around the world, such as Nagoya (Japan), Venice (Italy), San Joaquin Valley and Long Beach (California), and Houston (Texas). Likewise, Dhaka and Chittagong cities in Bangladesh are also subsiding, which is proven by a few other studies, but those studies did not show the factors, mechanism of subsidence, and rate of subsidence had anomalies as the rate of subsidence differ from each other.

Interferometric Synthetic Aperture Radar (InSAR), a satellite-based method, has become effective at mapping ground deformation across vast areas with mm-scale accuracy. These maps might offer crucial information on what causes subsidence by examining the parameters accountable to that ground motion jointly with other sources and in this study, I coupled SBAS-InSAR techniques, census reports of groundwater use, and population along with soil class to investigate the spatial relationship with those parameters. This study investigates the spatiotemporal characteristics of land motion between January 2018 and December 2021 over the city of Dhaka and Chittagong, located in Bangladesh.

The Small BAseline Subset algorithm is selected to minimize the spatial decorrelation problem. Sentinel-1 satellite data is used to generate a LOS (Line of Sight) velocity map. InSAR results showed that Dhaka and Chittagong city is subsiding at a significant rate along the LOS direction in some areas. The range of LOS velocity measured

is spatially varied in a complex way across both the study area. Patterns of subsidence correlate closely to geological settings and groundwater uses, which enabled us to find the recent land subsidence potentials and rates over the major urban areas of Bangladesh. This study also suggests monitoring the urban areas of Bangladesh using continuous observation techniques like the installation of GPS, proper investigation of lithology, and many more. At the same time, this study suggests through investigation of Chittagong city since the subsiding rate over the region is significantly high.

Keywords: SBAS-InSAR, Subsidence, Dhaka, Chittagong, Timeseries Analysis

Student Number: 2020-22032

Table of Contents

List of Figures

List of Tables

Chapter 1. Introduction

1.1 Research Background

Deltas are landforms created by depositing sediments carried by rivers as they flow into the mouth of a lake or ocean [1], a dynamic sedimentary environment that is also a living place for about half a billion people around the World [2]. Catchment developments, population, and economic growth introduce several problems to deltas. Around the world, out of 33 deltas, 24 are experiencing land subsidence, which is the delicate settling or quick sinking of the discrete portions of the ground surface due to natural processes like sediment loading combination, compaction, tectonic activity along with human activities like groundwater, hydrocarbon extraction [3, 4]. This leads to severe impacts when cities are located within these deltas, as land subsidence is a matter of great concern from a socioeconomic, environmental, protection, and food security viewpoint [5]. Coastal regions are the most prolific and valuable ecosystems on our planet and the thin transition between terrestrial and marine environments [6]. Around 60% of the world's major cities are located in coastal regions, and roughly 40% of the population of the planet lives within 100 kilometers of a coastline [7]. Many coastal cities are subsiding at a higher rate than the sea level rise around the World [8]. If the extent of subsidence in coastal areas continues at the recent rate, those coastal areas with be challenged by an environmental impact like flooding.

The Bengal Delta, which drains the whole Himalayas, is the biggest in the world. The delta is home to different plants, animal species, and humans. It is also a significant source of fresh water for the region, and geologically it is a lowland bounded by the Shillong

Plateau on the north, which lies between the collision zone of the Indian and Eurasia plate; the Burma Arc fold belt to the east; the Bay of Bengal on the south, and the Indian craton to the west have the uplifting characteristics [9]. The Ganges and the Brahmaputra, two Himalayan rivers, along with another non-Himalayan River, the Meghna, have built this delta in South-East Asia [10, 11].

Several other studies have proved that many areas worldwide suffer from subsidence due to fluid extraction, like China, Indonesia, and Italy [12-15]. It was proved that the leading cause of land subsidence was excessive groundwater pumping [16, 17]. The consolidation of the aquifer due to the overexploitation of groundwater results in rapid land subsidence. Variations could lead to the displacement of several centimeters in water storage in some cases. Throughout the world, manmade-induced subsidence and its impacts on the geological environment have been observed [18-20] along with those roads, bridges, and buildings that may be affected by subsidence within megacities like Mexico, Beijing, and Jakarta [21, 22]. To anticipate and mitigate those issues, it is essential to know the subsidence process to lower the magnitude of adverse impact and the contributing factors.

The Bengal Delta subsidence is not appropriately understood as only a few pieces of research had been carried out on a regional basis to measure the subsidence rate using magneto-stratigraphic dating, carbon dating, bore/well-logs, and geomorphic surveys [23, 24], which findings had the great extent of uncertainties and limited spatial extent. The analysis of river and tide gauges in the delta found subsidence of up to 7 mm/year [25]. Another study based on publicly available data (1987-2000) from Permanent Service for Mean Sea Level (PSMSL) founds a similar trend of subsidence with 11-20 mm/year along the coastline of the study area [26] biased by the examination of the 1977-2010 record of gauge using hourly data from

Bangladesh Inland Water Transportation Authority (BIWTA) [27]. Also, research was carried out to measure subsidence rate with GPS velocity measurement from 2003 to 2008 [28].

Subsidence phenomena up to cm to mm level precision are possible with GPS and leveling data with a higher temporal resolution. Still, these pointwise measurements fail to provide spatial variability to identify the occurrence and magnitude of local small-scale subsidence, especially for regions without monitoring sensors [29-32]. Interferometric Synthetic Aperture Radar (InSAR), on the other hand, is an active satellite remote sensing method capable of detecting millimeter to centimeter-level movements of the Earth's surface using backscatter phase information but having lower temporal resolution [33, 34]. Therefore, combining InSAR, GPS, and other data sources by incorporating their spatial and temporal resolution properties and sensitivity to different components of ground motion is more capable of precise ground movement measurement.

In terms of the remote sensing approach, exploitation of C-band and L-band InSAR techniques was applied earlier for investigating the subsidence rates in Bangladesh (on a local scale), especially in Dhaka city [11, 35]. However, studies were done with L-band InSAR techniques measured an average rate of subsidence of 3.8 mm/year largely differs from what was found at about 12.4 mm/year with GPS measurement in Dhaka. In terms of methodology, this study used conventional InSAR techniques (affected by phase noise), which have fewer advantages than Persistent Scatter Interferometry (PS-InSAR) and Small Baseline (SBAS) due to the lack of a large number of images. On the other hand, the study did not investigate the factors or parameters correlated with the subsidence.

This study seeks to measure the recent rates of land subsidence along Dhaka and Chittagong city of Bangladesh using the SBAS InSAR technique. It is hypothesized that the current rate of land subsidence

is higher than the previous study, and the subsidence velocity is primarily controlled by local geology and fluid extraction. The intellectual merits of this study are the combination of InSAR and factors affecting the subsidence along major urban areas of Bangladesh. To that end, this study centered on the first-time satellite-based detection and monitoring of subsidence of major urban areas of Bangladesh induced by a variety of natural and anthropogenic phenomena, which will give an insight into the causes of subsidence and the recent rate of subsidence. With this work, I used Small Baseline Subset Interferometric Synthetic Aperture Radar (SBAS-InSAR) method to scrutinize the subsidence evolution along major urban areas of Bangladesh. The primary focus of this study has twofold: (1) To prepare and preprocessing spatial influencing factors for analyzing InSAR-derived urban subsidence in Bangladesh (2) To identify major factors of subsidence in urban areas using geo-statistical analysis. Satellite images are collected from the Alaska Satellite Facility (ASF) of the Sentinel-1 satellite and processed using the method detailed in the methodology section to calculate current subsidence velocity (LOS). Finally, those measurements are used to map the subsidence rate in the LOS direction within our area of interest. The maps are first visually inspected for spatial patterns that correlate with natural and anthropogenic influences, like geology (Soil class) and groundwater withdrawal (Dependency on groundwater as drinking water sources); also, statistical analysis is executed to prove the relationship with factors hypothesized with this study.

1.2 Thesis Outline

Chapter 2 introduces the study area and the datasets used for this study.

Chapter 3 denotes the detailed procedure of the study to retrieve

the subsidence information and statistical analysis methods.

Chapter 4 describes the detection performance of the study and visual interpretation, statistical analysis of InSAR results, and

Chapter 5 provides a discussion of the outcomes of this study.

Chapter 6 is the conclusion of the dissertation.

Chapter 2. Study Area and Data Selection

2.1 Study Area

2.1.1 Geographical Location

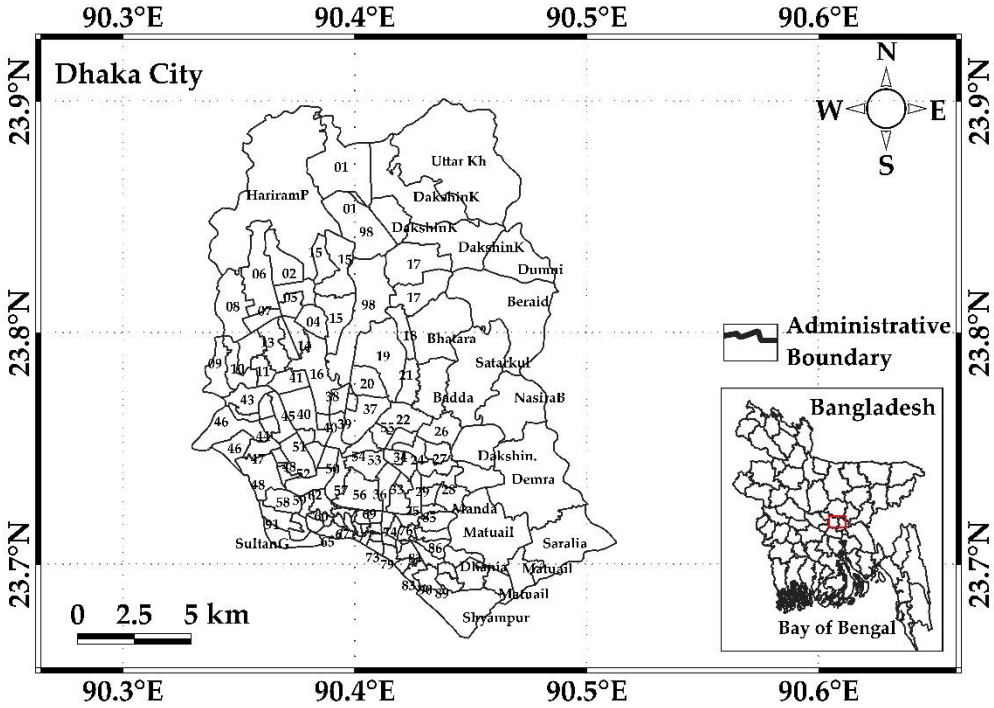

Figure 2.1 Study Area, Dhaka City.

Bangladesh's capital and largest city, Dhaka, is situated in the country's central region between the longitudes of 90°19′10.37″ and 90°31′1.61″ and the latitudes of 23°40′49.9″ and 23°54′46.5″. It has a total area of 306 square kilometers (Figure 2.1). Due to population migration from the countryside and townships, Dhaka city has been observing significant growth in its population over the last three decades [36]. Dhaka city is encompassed by the floodplains from the

Ganges, Jamuna, and Meghna rivers and is surrounded by Buriganga, Turag, Balu, and Shitlakhya [37].

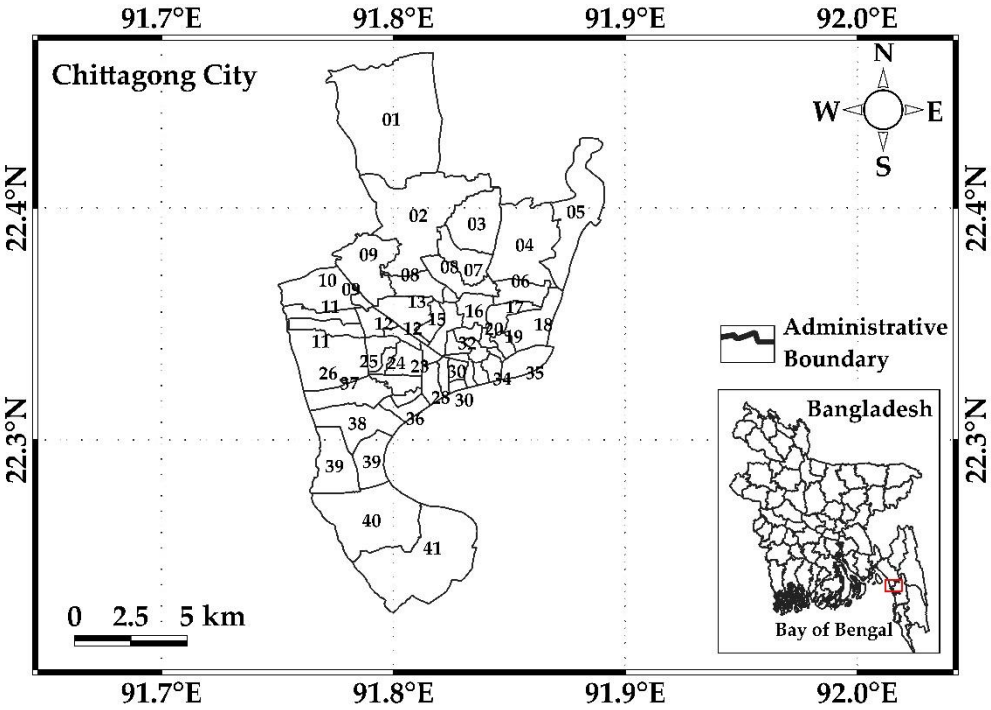

Figure 2.2 Study Area, Chittagong City.

Chittagong is the second largest city of Bangladesh, located in the southeast region of Bangladesh; it lies between longitudes 91°7′ E to 92°14′ E and latitude 21°54′ N to 22°59′ N, covering an area of about 155 square kilometers (Figure 2.2). It is situated on the north bank of the river Karnaphulli between the Chittagong Hill Tract and the Bay of Bengal, with a population of about 2.5 million [38]. Chittagong city also includes the Chittagong seaport which is the largest seaport in Bangladesh. It is located on the bank of the Karnaphuli River and is the core part of countries dependent on the Bay of Bengal.

2.1.2 Geology of the Study Area

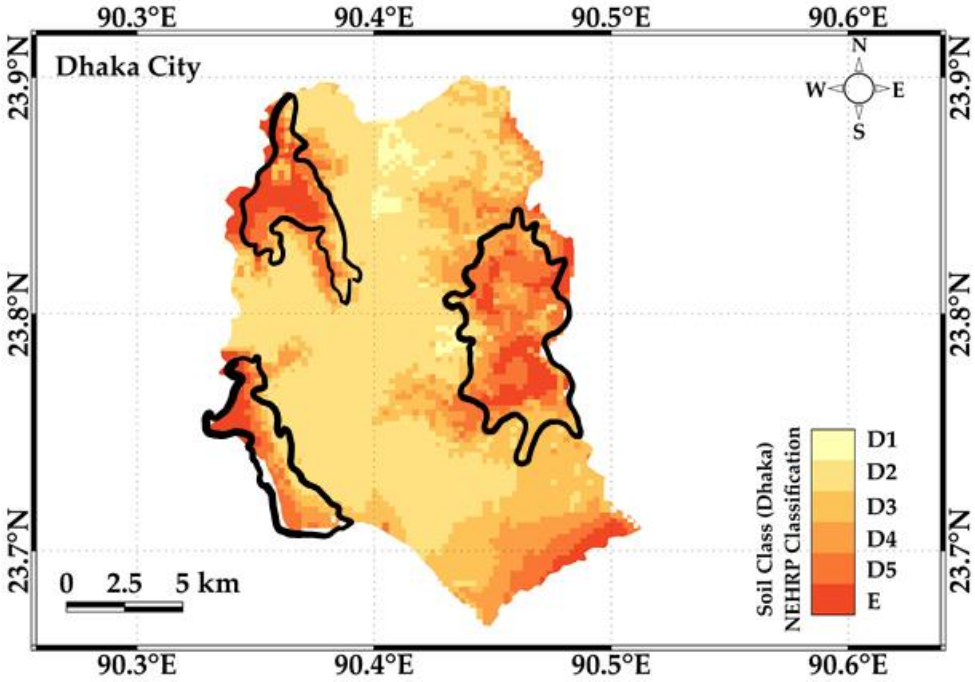

Figure 2.3 Soil Classification of Dhaka city (D1, D2 refer to stiffest soil units which are termed tulus deposits, D3 and D4 refer to fewer stiff units compared to D1 and D2, composed of sands, silts, and clay termed floodplains and D5 is less stiff than that of D3 and D4, and Class E refers to artificial deposits).

Dhaka city is spread out on a low-lying Holocene floodplain and a high Pleistocene terrace (Madhupur terrace). The geology of the city broadly can be divided into six distinctive units. They are 1) Pleistocene terrace deposit, 2) Holocene terrace deposit 3) Holocene alluvial valley fill deposit 4) Holocene alluvium 5) Holocene channel deposit and 6) Artificial fill.

The National Earthquake Hazards Reduction Program (NEHRP) program now recognizes the association between the shear wave

velocity of the top 30 m of sediments and/or rocks and ground motion amplification. The surface geology of Dhaka is divided into six separate classes (Figure 2.3), according to NEHRP class from the Comprehensive Disaster Management Programme [2009] D5 refers to a unit that is significantly less stiff than classes D3 and D4, whereas D1 and D2 are stiffest units, relating to Madhupur clay and a localized tulus deposit. D3 and D4 are fewer stiff units, corresponding to Holocene alluvial (floodplain) sand, silt, and clay. Holocene marsh sediments and more recent artificial fill (>500 years) make up most of Class E.

According to geology, the Chittagong region is part of the Bengal Foredeep of the Bengal Basin, where Neogene strata with a well-developed shale and sandstone alternation are found.

The area fills a sizable space between the Arakan Yoma Folded System and the Hinge Line. Floodplain deposits with various depressions, such as ditches, marshy terrain, etc define the region's topography. The study area is generally elevated between −8.8 and 4.395 meters. In the Foredeep region, the basement rock is likely found between 12 and 15 kilometers below the surface. The area under investigation is on the folded flank of the Foredeep, which encompasses many of Chittagong and the Chittagong Hill Tracts' sub-meridian structures. The slight sloping to the south and west [39].

The region's surface geology features a large variety of geologic units. Geomorphic location dominates and controls the distribution and order of the geologic units. There are two main trends in the surface geology of the Chittagong City region. In the southern portion of the research region, between the Karnaphulli River to the east and south and the Bay of Bengal to the west, Quaternary sediments were exposed.

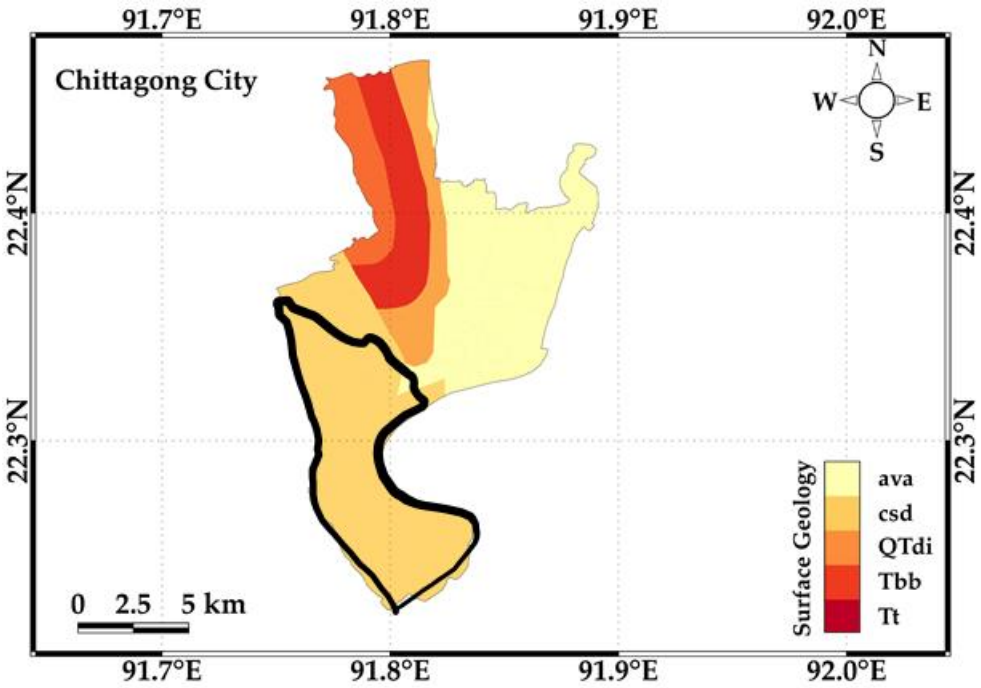

Figure 2.4 Soil Classification of Chittagong City (ava is valley alluvium and colluvium, csd is beach and dune sand generally refers to coastal deposits, QTdi is Dihing Formation having sandstone, claystone, and siltstone (Pleistocene and Pliocene), Tbb is boka bil formation consist of siltly shale/shale, siltstone, and sandstone (Neogene), and finally Tb refers to bhuban formation composed of shale, sandy shale and siltstone (Miocene)).

The northern portion of the research area featured the most exposed tertiary deposits. On the western and eastern edges of the northern half, fill deposits from the Piedmont and valleys cover the surface. Surface geology serves as the primary foundation for the concept of the subsurface geology of the study area.

2.1.3 Hydrology of the Study Area

The Madhupur Clay, also known as the Dupi Tila aquifers, sits on

top of a series of sands that range in size from fine to coarse. The Dupi Tila Formation's fine- and medium-grained sands at the top grade into medium- and coarse-grained sands with gravels as they descend to the base. The Dupi Tila system is split into two aquifers by a discontinuous clay layer: an upper, fine-grained aquifer (the upper Dupi Tila aquifer 1), which is 40–50 m thick, and a lower, coarser aquifer (the upper Dupi Tila aquifer 2), which is 80 m thick. Recently, boreholes conducted for exploration beyond 200 m depth have breached the underlying clay layer. Overlying a deeper sequence of sands that is more than 100 m deep is the basal clay, which is 10 to 15 m thick.

Chittagong's hydrogeology is tectonically and structurally regulated. The aquifer geometrical patterns undergo regular changes on a local level. The area that was uplifted quickly due to tectonic compression is characterized by a steep gradient and a high sediment supply. The sides of the flood plain, on the other hand, are routinely filled upward and are distinguished by a prevalence of muddy overbank deposits. Poor to fair aquifer conditions with changing piezometric levels or heads and low to extremely low permeability was the result of this. Since individual wells have been dug to these depths, it is not well understood how thick the deposits in the floodplain are, but they are more than 250–300 m thick. The depth is widely thought to be far greater, though sediment layers with larger grain size.

2.2 Single Look Complex (SLC) Data Selection

In this study, descending direction SLC (Single Look Complex) datasets for Sentinel-1 satellite were collected from Alaska Satellite Facility that downlinks, processes, archives and distributes remote-sensing data to the scientific user all around the world whose mission is to make remote-sensing data accessible. Descending (Des) orbit

path number 150, and 77 covering the capital of Bangladesh, Dhaka city, and the second largest city of Bangladesh Chittagong from 2018 to 2021 is used for the study. Coverage of the SLC scene on the map is given in figure 2.5.

Figure 2.5 Map of the study area, bounding box covers the scene for Sentinel-1 satellite of the study area.

Furthermore, details on Sentinel-1 SLC scenes are given in the following tables, which focus on a very basic description of the SLC data used for this study separately for both the major urban area of Dhaka and Chittagong of Bangladesh in tables 2.1 and 2.2.

Table 2.1 Sentinel-1 SLC Data Description Dataset 1:

Description	Properties
Path	150
Frame	510
No. of Scene	89
Period	2018-2021
Orbit	Descending
SLC Spatial resolution	(20 x 5) m
Center inc. angle	39.41
Range looks	9
Azimuth looks	3
Polarization	VV

Table 2.2 Sentinel-1 SLC Data Description Dataset 2:

Description	Properties
Path	77
Frame	520
No. of Scene	81
Period	2018-2021
Orbit	Descending
SLC Spatial resolution	(20 x 5) m
Center inc. angle	37.10
Range looks	9
Azimuth looks	3
Polarization	VV

2.3 Groundwater Use and Population Data:

The population and housing census is the only source of trustworthy and comprehensive statistics on Bangladesh's population numbers as well as significant socioeconomic and sociodemographic

features. The population and housing census collect data on the geographic and administrative distribution of the country's population and households, as well as the demographic and socioeconomic characteristics of all citizens. The census data is categorized, tabulated, and disseminated so that researchers, administrators, policymakers, and development partners can utilize it to create and implement various multi-sectoral development projects at the national and community levels.

In this study, we collected the groundwater use data for Dhaka and Chittagong city from the last population and housing census report of Bangladesh that took place in 2011. For administrative purposes, both Dhaka and Chittagong city are subdivided into small units called a ward. Data collected on population, and groundwater use data for both the city for each administrative unit ward. Appendix 1 describes the details data of Dhaka city and Appendix 2: describes the details data of Chittagong city's population and census reports relevant to this study.

2.4 Subsurface Sedimentary Sequences (Chittagong):

A feasibility study named "Multilane Road Tunnel under the River Karnaphuli, Chittagong, Bangladesh" was done during the construction of a tunnel in Chittagong. They used the lithologic cross-section data during their study. Though we tried to access those data but failed. So, we collected the 3D diagram of the lithologic cross-section which had information on lithology up to a depth of 300m. Further, analyzed the image data to convert those to clay (%) data for the Chittagong study area. Figure 2.6 shows the lithologic cross-section of the study area Chittagong along with the map of the wells, and the direction of clay proportion extraction (Clay proportion is extracted along the yellow arrow shown in figure 2.6). Clay proportion data extracted from the image analysis of lithologies are given in table 2.3

Table 2.3 Chittagong City Subsiding area's clay Information:

Chittagong City		
Wells	Clay %	Sand %
Navy-17	29.65	70.35
EPZ-2	53.42	46.58
Ward-40 (Analysis)	54.48	45.52
Ward-39 (Analysis)	53.33	46.67
Ward-38 (Analysis)	50.38	49.62

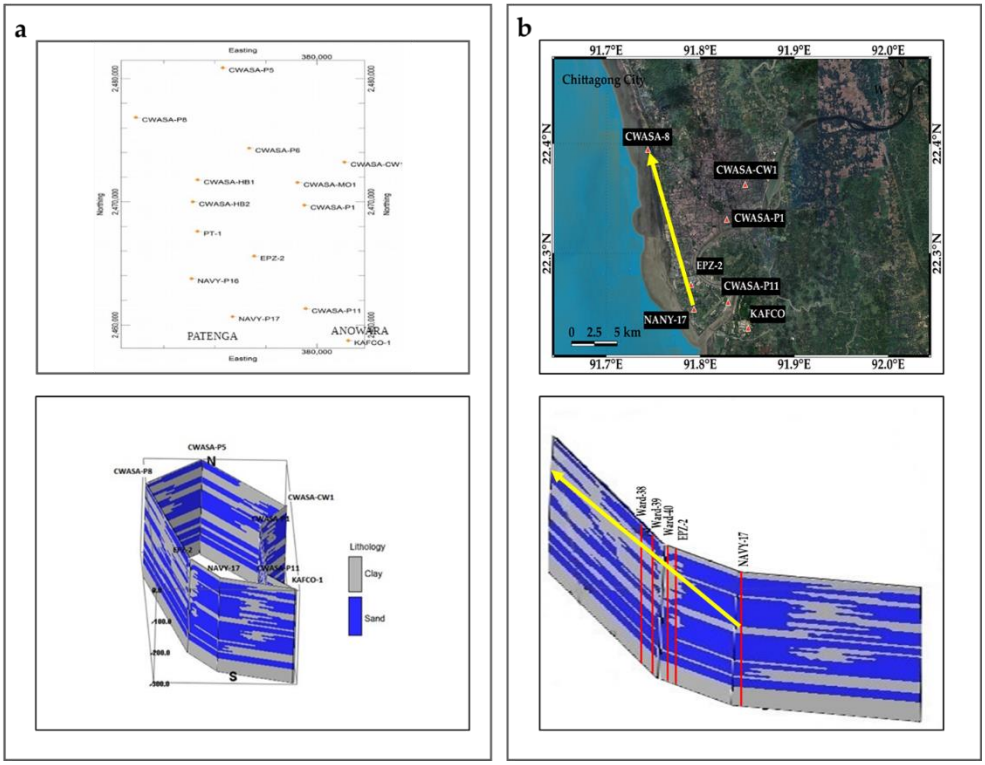

Figure 2.6 (a)Lithologic diagrams of Chittagong city – Anowara area down to the depth of 300 m based on CWASA and other logs [39] . (b) Area of interest modified form (a).

2.5 Impact of Sedimentary Sequence on Subsidence:

The primary contributors to land subsidence brought on by groundwater pumping are fine-grained sediments especially clays and silts within an aquifer system. They are composed of platy grains by nature. Fine-grained sediments frequently have random orientations when they are first deposited. There is plenty of space between these randomly arranged sediment particles for water storage. However, such randomly orientated sediments are reorganized into stacks when groundwater levels drop too low levels. To store water, these stacks have less space between them. The impact of clay on subsidence has been proved by different studies and the science behind the subsidence with graphics is as follows [40]

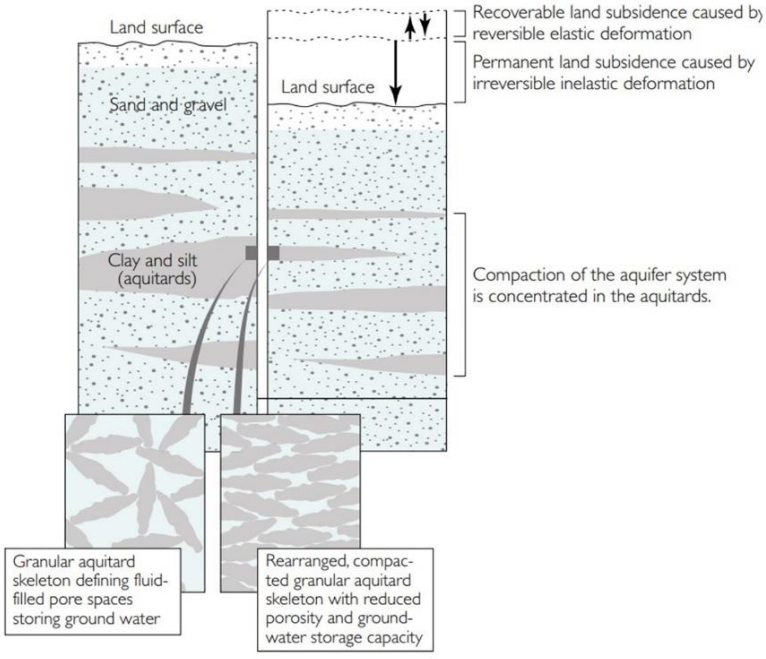

Figure 2.7 Impact of clay on land subsidence [40]

2.6 Data Normalization and Standardization:

Normalization:

This process is also called Min-Max Scaling. In this process, transformation of data is done in such a way that the values range from 0 to 1. This can be done by subtracting the minimum value from each data point and then dividing it by the range. The range is calculated by subtracting the minimum value from the maximum value. This ensures that all our data points are within the range of 0 to 1.

$$X_{norm} = \frac{X - \min(X)}{\max(X) - \min(X)} \qquad 2.1$$

Where, X_{norm} corresponds to normalized data, X is the data before normalization, max(X) implies maximum value of X and min(X) implies minimum value of X.

Figure 2.8 Data normalization overview.

Standardization:

The practice of putting different features on the same scale is

known as data normalization. To put it another way, standardized data is created by rescaling the attributes so that their mean is 0 and standard deviation is 1.

At the same time as our data had categorical values (for Dhaka city), there is a need of utilizing any technique so we used the dummy variable technique to remove the anomalies in our results.

$$X_{Stand} = \frac{X - \text{mean}(X)}{\text{std. dev}(X)} \qquad 2.2$$

Where, X_{stand} corresponds to standardized data, mean(X) imples the mean value of X and finally std. dev(X) is the standard deviation of X.

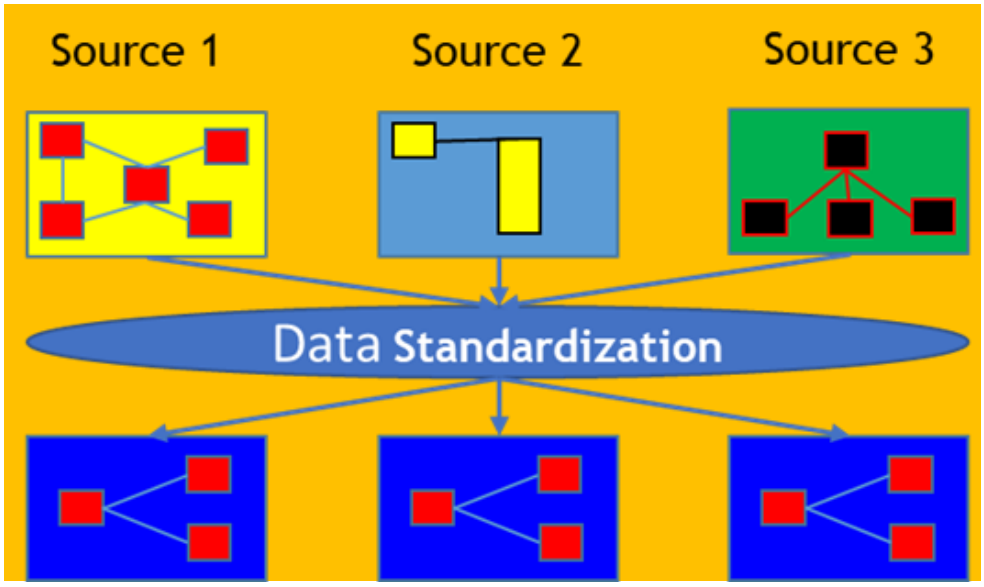

Figure 2.9 Data standardization process.

Chapter 3. Methodology

This chapter offers a brief overview of the methodology of Synthetic Aperture Radar, Interferometric Synthetic Aperture Radar, and Time-series Interferometric Synthetic Aperture Radar techniques like SBAS InSAR. During this study, all the above principles is deployed to access the subsidence of two major cities located in Bangladesh.

3.1 Synthetic Aperture Radar

Synthetic Aperture Radar (SAR) is a microwave imaging device with the ability to penetrate clouds and operate both during the day and at night. As a side-looking radar antenna has the arrangement to eliminate the ambiguity of backscatter from both sides of the satellite track, it actively illuminates the ground with electromagnetic pulses with a microwave frequency (0.3-300 GHz, 1000-1 mm [41]. Synthetic Aperture Radar (SAR) involves a coherent airborne side-looking pulsed radar system that utilizes its flight path to simulate a profoundly large antenna and microwave radiation is transmitted to the ground to illuminate the target. As a result, a synthesized larger antenna coverage becomes available [42, 43]. The basic geometry of the side-looking SAR Imaging system is given in a sketched figure 3.1

The direction of radar illumination is called the range direction whereas the moving direction of a satellite is called the azimuth direction. The antenna receives the backscattered signal from the target. With this geometry and using the speed of light, the range gets measured.

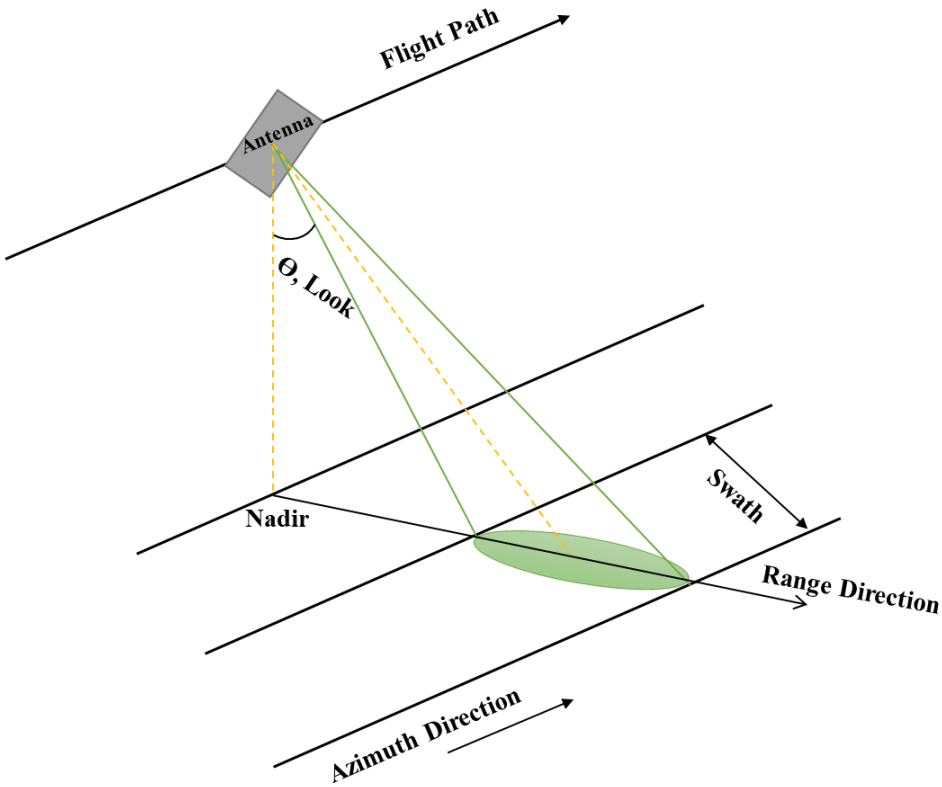

Figure 3.1 Typical SAR imaging geometry.

The microwave energy scattered back to the radar system gets measured. All the radar-returned signals are processed to determine the properties of the target. There are variations in returned signals based on the distance of the target. As a result, by measuring the time variations between the transmission and reception of pulse t, the range between the sensor/radar and the target is calculated as.

$$R_S = \frac{ct}{2} \qquad 3.1$$

Where Rs is the slant range distance, c is the speed of light and t is the time difference between transmission and reception of a pulse.

3.2 Interferometric Synthetic Aperture Radar (InSAR)

A Synthetic Aperture Radar (SAR) image is the precise observation of the amplitude and phase data of echo recorded at the satellite. A pulse of microwave radiation is emitted from the satellite towards the ground and some of it is scattered back to the satellite, which gets recorded as SAR images. As the scatter of different distances travels a different path to the satellite, the delay of transmission and reception of the signal becomes different. Due to the sinusoidal nature of the transmitted signal, this phase delay is precisely correspondent to the phase change of conveyed and received signals. SAR interferometry is the technique of imaging surface and ground displacement using the phase values of two or additional SAR images. In this method we equate assuming that we can correct the satellite's location, the phase from two different passes of the same satellite over the same point of ground; the difference in phase between the two passes must be proportional to the change in distance between the satellite and the ground.

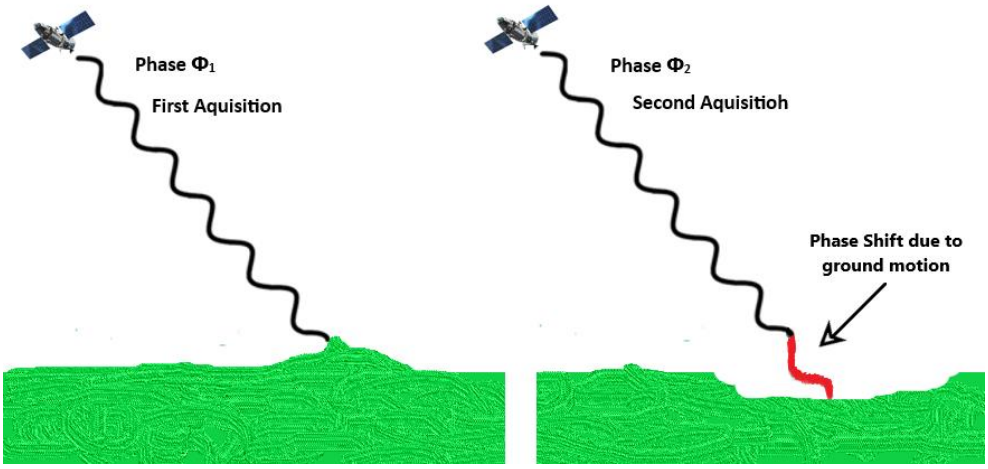

Figure 3.2 Schematic cartoon of how InSAR works.

Two complex SAR image taken over the same region either by two antennae of a single satellite or during the repeat pass of the same satellite gets cross-multiplied to generate an interferogram. This can be expressed as follows

$$\varnothing_{int} = \frac{4\pi\Delta R}{\lambda}, \ \Delta R = R2 - R1 \qquad 3.2$$

Where R1 and R2 are the two line of sight distances for the first and second pass of the satellite and ΔR is the difference between R1 and R2. The distance between two satellite tracks that are perpendicular to the target's slant range and height is known as the perpendicular baseline, or B_{prep}. It's important to note that we can only gauge the movement of the ground relative to the satellite in the direction of line of sight.

The interferometric phase is the contribution of different sources and they are as the following equation.

$$\varnothing_{int} = \varnothing_{defo} + \varnothing_{topo} + \varnothing_{orb} + \varnothing_{atm} + \varnothing_{noise} \quad 3.3$$

The topography of the earth $\varnothing_{topo}$ is the main contributor in the interferometric phase, $\varnothing_{orb}$ is the inaccuracy of information of the orbit, the ground deformation between two image acquisitions, $\varnothing_{defo}$, the phase delay in transmission and reception of SAR signal $\varnothing_{atm}$ is the atmospheric noise, and finally, due some other issues like temperature, a certain extent of noises get introduced with the interferometric phase information.

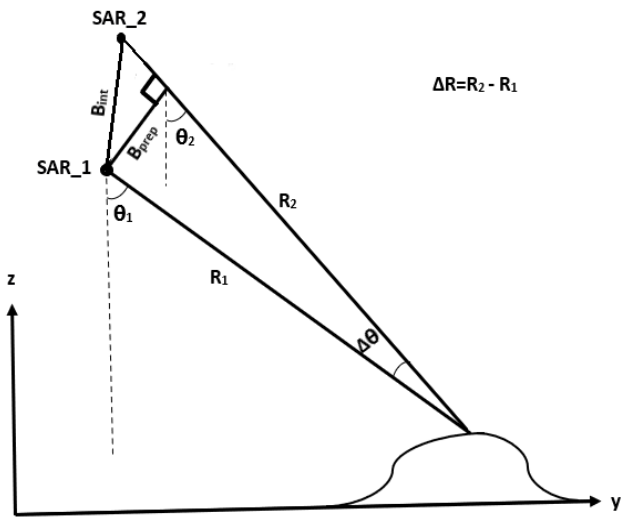

Figure 3.3 Schematic cartoon of SAR Interferometry geometry

Topography of the earth $\varnothing_{topo}$ can be derived using the InSAR viewing geometry as described in [44, 45] and can be defined as

$$\varnothing_{topo} = \frac{4\pi B prep\ \acute{h}}{\lambda R sin\Theta} \qquad 3.4$$

When SAR satellites are not in a position where they are parallel to each other, the phase difference of two points is related to the range difference ΔR. With this property higher density, interferometric fringes get appear even though the earth's surface is flat which requires to be removed from the total interferometric phase and this processing is termed interferogram flattening.

Target's positional change in two SAR acquisitions along the line of sight (LOS) direction is displacement and in phase format termed as $\varnothing_{defo}$, is given as

$$\varnothing_{topo} = \frac{-4\pi d}{\lambda} \qquad 3.5$$

In the differential interferometry technique, deformation $\varnothing_{defo}$ gets computed based on parameters listed in equation 3.3. The calculated phase for topography, atmosphere, and orbit becomes subtracted from the interferometric phase, so the final remaining of the interferometric phase becomes phase due to deformation and some noises in wrapped format.

Figure 3.3 shows the outline of the InSAR processing flowchart to generate a displacement map from SAR images. Firstly, two SAR images are co-registered using the information of orbit and DEM (Digital Elevation Model), and the interferogram gets generated by subtracting the phase of the secondary or slave image from the phase of the reference or master scene. By removing the topographic contribution to the interferogram using DEM, a differential interferogram gets generated. Initially, the phase is wrapped which required it to be unwrapped with an unwrapping tool. The 2π modulo gets converted into ground displacement and then geocoded to find

the exact location of deformation at each pixel. The differential interferogram sometimes gets affected by noise sources and other decorrelation sources. Conventional Differential Interferometry (D-InSAR) is unable to measure deformation signals because of low coherence caused by a larger perpendicular baseline, temporal decorrelation caused by phase delay variations caused by the atmosphere, weather, and surface changes over time, such as seasonal vegetational changes.

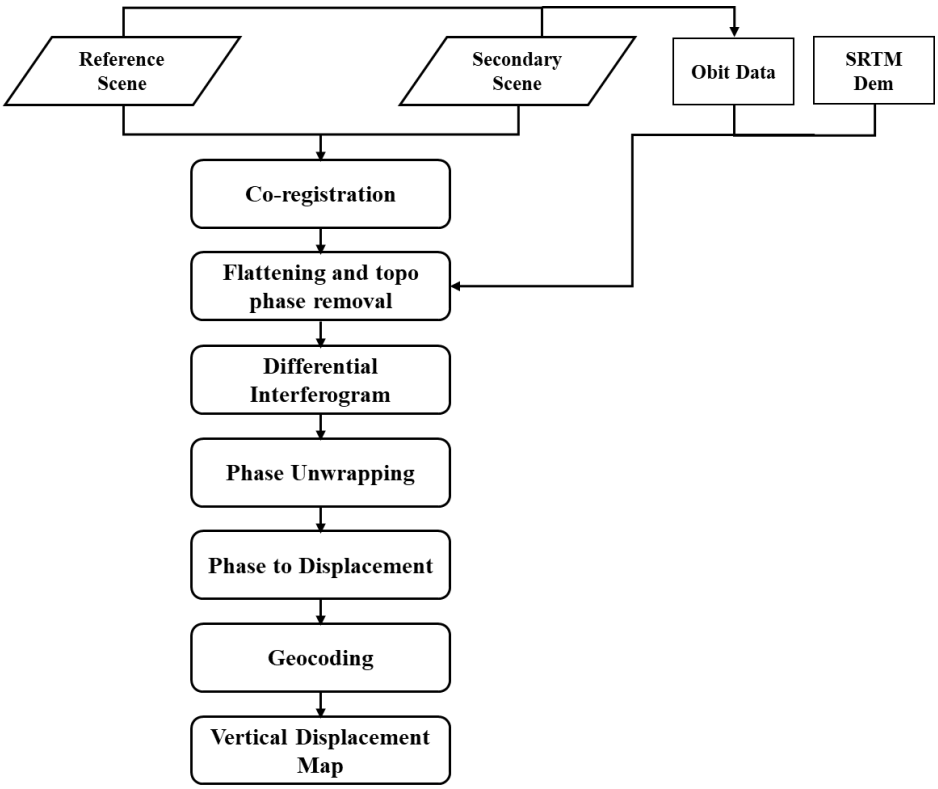

Figure 3.4 Flowchart of differential interferometry processing.

Coherence γ is the measure of the correlation between the phase measured at the different (spatial and temporal) points of a wave. The

coherence is determined as a quality indicator of the phase difference between two SAR acquisitions at that point. According to a specific pixel in a differential interferogram, which can be described as [46],

$$\gamma = \frac{E\{S_1 \bullet S_2^*\}}{\sqrt{E\{S_1 + S_1^*\} \bullet E\{S_2 \bullet S_2^*\}}} \qquad 3.6$$

Where, E is the expected value of complex SAR images S_1 and S_2, S_1^* and S_2^* are complex conjugates of SAR scenes 1 and 2. The measurement of coherence ranges from 0 to 1, where pixels having values close to 1 are considered as mostly correlated or coherent, on the other hand, pixels having values reverse for 0 are considered as decorrelated to incoherent pixels. Among thermal, spatial, and temporal coherence, temporal coherence has the most important where the target is to measure the temporal changes of ground motion. Due to a longer temporal baseline, there is a chance of decreased coherence and similar to a longer perpendicular baseline causes the loss of spatial coherence. To overcome this issue to an extent stacking of D-InSAR along the time which is also termed time-series SAR interferometry.

3.3 Time-series SAR interferometry

The decorrelation issues in conventional D-InSAR were the key to searching for some other approach for differential SAR Interferometry. As an approach to eliminate the decorrelation, the time-series InSAR technique was developed which utilizes a series of SAR images to measure the ground displacement over the time of image acquisition. This is done based on different baseline configurations. A framework of time-series interferometry named Persistent Scatterers Interferometry (PSI) was proposed by [47]. In

the PSI technique, a stack of interferograms having a single reference gets generated to identify the coherent pixels termed PS (Permanent Scatterer) can minimize the decorrelation problem in conventional D-InSAR. Following that, Small Baseline Subset (SBAS) InSAR technique was proposed by [48] with multilooked and unwrapped interferograms which get generated by small temporal and perpendicular baseline. There are several approaches to process SBAS-InSAR processing.

3.4 SBAS-InSAR

SBAS or Small Baseline Subset InSAR analysis starts with considering the acquisition of an N+ 1 SAR image of the same area and at a different time (t0,...,tN) and assuming that each image may interfere with at least another image; which implies every small baseline subset is composed of minimum two images. So, the total number of possible differential interferograms, for example, M will satisfy the following equation.

$$\frac{N+1}{2} \leq M \leq N\left(\frac{N+1}{2}\right) \qquad 3.7$$

The expression of the generic j-interferogram computed at a pixel having azimuth and range coordinate (x,r) with acquisition at time tA and tB is, according to Berardino et al (2002) as follows.

$$\delta\phi_j(x,r) = \phi(t_B,x,r) - \phi(\mathrm{t}_A,x,r)$$

$$\approx \frac{4\pi}{\lambda}[d(t_B,x,r) - d(\mathrm{t}_A,x,r)] \qquad 3.8$$

Here, $d(t_B,x,r)$,$d(t_A,x,r)$ are line-of-sight (LOS) cumulative deformation at time t_A and t_B with respect to t_0 considered as reference

and λ transmitted signals central wavelength. So, we can identify $d(t_i,x,r)$ with i= 1, …., N as the wanted deformation time-series the deformation is associated with the phase component;

$$\phi(t_i, x, r) \approx \frac{4\pi d(t_i,x,r)}{\lambda} \qquad 3.9$$

3.5 ISCE interferogram stack processing

ISCE is an Interferometric SAR (InSAR) Scientific Computing Environment (ISCE) for geodetic image processing that is both flexible and extendable. ISCE was built from the ground up to be a geophysical community tool for generating stacks of interferograms that lend themselves to various forms of time-series analysis, with accuracy, extensibility, and modularity.

Sentinel-1 SLC data are freely available through Alaska Satellite Facility (ASF) for research and education purposes. After downloading the SLC data further processing for interferogram stack generation is done using ISCE (Interferometric synthetic aperture radar Scientific Computing Environment). Figure 3.4 given below, is a flowchart for interferogram stack generation using ISCE software.

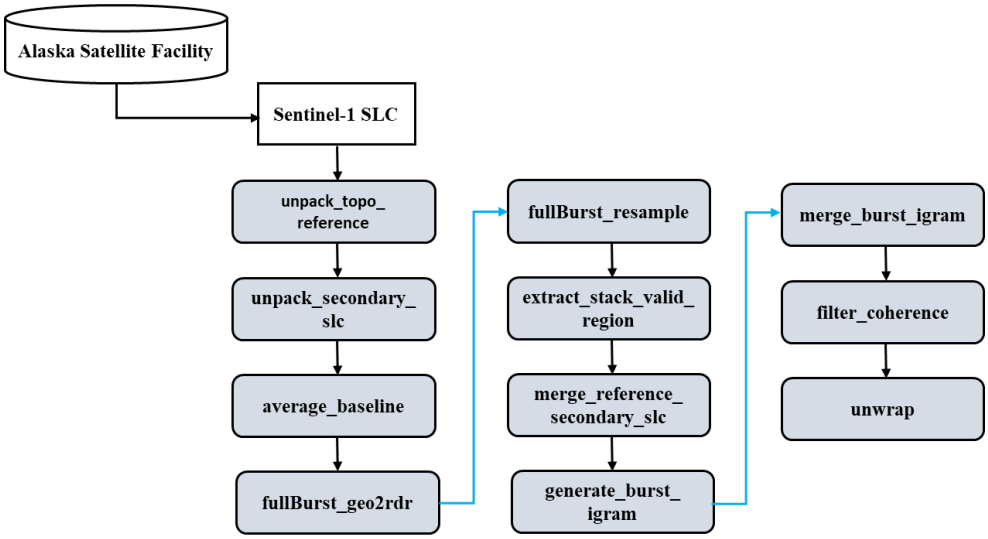

Figure 3.5 Flowchart of interferogram stack processing with Sentinel-1 SLC data.

This stack of interferograms works as the input data for SBAS-InSAR processing using MintPy (Miami InSAR time-series software in Python).

3.6 Mintpy SBAS-InSAR processing

Mintpy SBAS-InSAR processing starts with the interferogram stack co-registered to a common SLC scene and which is already unwrapped. In the first step, if there is any interferogram having a spatial coherence less than the predefined value or unwrapping error, the modification of the network is made. Then the reference points are selected using the prior knowledge of the study area. An unwrapping error correction is done in MintPy if it is defined in the input file. Bridging and phase closure are two methods in unwrapping error correction.

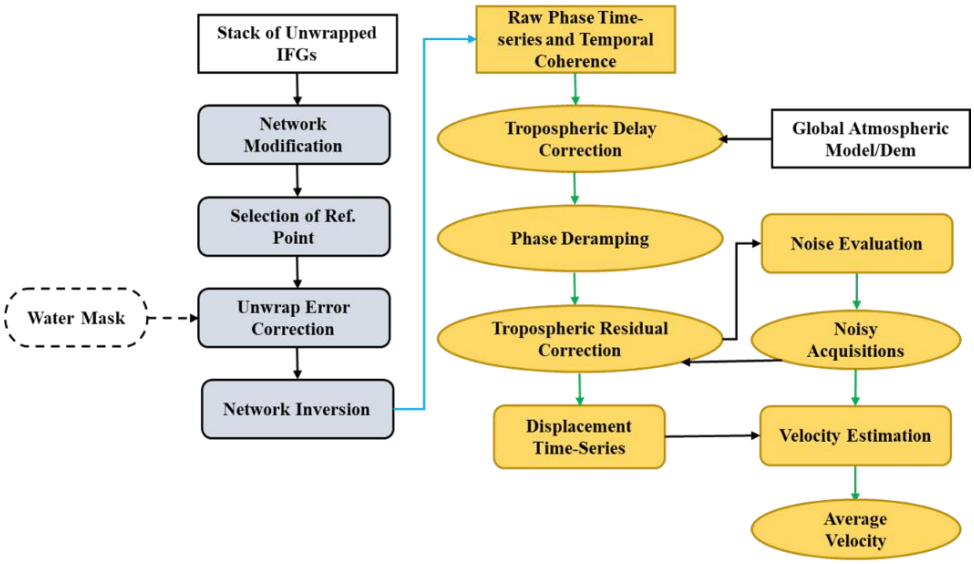

Figure 3.6 Flowchart of Mintpy SBAS-InSAR processing modified from [49].

After the phase unwrapping error correction, the network inversion starts. In this step, the pixels in shallow and water bodies are masked out with a shallow mask and water body mask and then the tropospheric delay correction takes place aided by the global atmospheric model or dem. Due to orbital errors, tropospheric and ionospheric delay residual the phase ramp causes. In the phase deramping step, the removal of the ramp is possible. Next is the tropospheric residual correction and displacement time-series generation from which the velocity gets estimated, and finally, the average velocity can be obtained.

3.7 Investigation of Spatial Relationship

Regression analysis allows us to investigate, examine, and explore the spatial relationship which explains the factors behind the observed

spatial pattern within the study area. This also allows us to have a better understanding of the phenomena taking place with our datasets, where the basic objective is to build a prediction model with consistency and accuracy. Out of which OLS or ordinary least square is the best known of all regression techniques and the starting point of spatial regression analysis. It gives a global model of the variable that we are trying to understand or predict. For a better understanding of regression analysis, we need to know a few key terms and the basic concept of regression statistics.

3.7.1 Ordinary Least Squares

OLS Regression Equation: A regression equation is a mathematical formula that uses the explanatory or independent variables to best predict the dependent variables [50] which we are trying to investigate. In the regression equation, independent and dependent variables notation is used as X and Y where each independent variable is associated with a regression coefficient which describes the strength and the sign of that variable's relationship to the dependent variable. An example of a regression equation is given below for a better understanding.

$$y_i = \beta_0 + \beta_1 x_{1i} + \beta_2 x_{2i} + \beta_3 z_{1i} + \beta_4 z_{2i} + \beta_5 z_{3i} + \varepsilon_i \qquad 3.10$$

Where, y_i is estimated LOS velocity, β_0, β_1, β_2, β_3, β_4 and β_5 are co-efficient of groundwater (X_1), population (X_2) and dummy variables (z_1, z_2 and z_3 for moderate, low stiff and artificial fill of soil). And Where, i= 1, 2, 3, ⋯ ⋯ ⋯ ,n. When i=1, 2, 3, ⋯ ⋯ ⋯ ,n then

$$y_1=\beta_0+\beta_1 x_{11}+\beta_2 x_{21}+\beta_3 z_{11}+\beta_4 z_{21}+\beta_5 z_{31}+\varepsilon_1$$

$$y_2=\beta_0+\beta_1 x_{12}+\beta_2 x_{22}+\beta_3 z_{12}+\beta_4 z_{22}+\beta_5 z_{32}+\varepsilon_2$$

$$y_3=\beta_0+\beta_1 x_{13}+\beta_2 x_{23}+\beta_3 z_{13}+\beta_4 z_{23}+\beta_5 z_{33}+\varepsilon_3$$

.

.

.

$$y_n=\beta_0+\beta_1 x_{1n}+\beta_2 x_{2n}+\beta_3 z_{1n}+\beta_4 z_{2n}+\beta_5 z_{3n}+\varepsilon_n \qquad 3.11$$

Using matrix notation which can be written as

$$\begin{bmatrix} y_1 \\ y_2 \\ y_3 \\ . \\ y_n \end{bmatrix} = \begin{bmatrix} 1 & x_{11} & x_{21} & z_{11} & z_{21} & z_{31} \\ 1 & x_{12} & x_{22} & z_{12} & z_{22} & z_{32} \\ 1 & x_{13} & x_{23} & z_{13} & z_{23} & z_{33} \\ 1 & . & . & . & . & . \\ 1 & x_{1n} & x_{2n} & z_{1n} & z_{2n} & z_{3n} \end{bmatrix} . \begin{bmatrix} \beta_0 \\ \beta_1 \\ \beta_2 \\ \beta_3 \\ \beta_4 \\ \beta_5 \end{bmatrix} + \begin{bmatrix} \varepsilon_1 \\ \varepsilon_2 \\ \varepsilon_3 \\ . \\ \varepsilon_n \end{bmatrix} \qquad 3.12$$

$$Y=X\beta+\varepsilon$$

$$\varepsilon=Y-X\beta \qquad 3.13$$

In the ordinary least square method

$$\sum(\varepsilon_i)^2=\sum(\varepsilon_1)^2+\sum(\varepsilon_2)^2+\cdots\ \cdots\ \cdots\ +\ \sum(\varepsilon_n)^2$$

$$=\begin{bmatrix}\varepsilon_1 & \varepsilon_2 & \varepsilon_n\end{bmatrix}.\begin{bmatrix}\varepsilon_1 \\ \varepsilon_2 \\ \varepsilon_n\end{bmatrix}$$

$$=\varepsilon'\varepsilon \qquad 3.14$$

Substituting ε value in equation (3.14)

$$=(Y-X\beta)'(Y-X\beta)$$

$$=(Y'-\beta'X')(Y-X\beta) \qquad \text{as } (AB)'=B'A'$$

$$=Y'Y-\beta'X'Y-Y'X\beta+\beta'X'X\beta$$

$$=Y'Y-2\beta'X'Y+\beta'X'X\beta$$

$$\frac{\partial}{\partial\beta}\left(\sum(\varepsilon_i)^2\right)=\frac{\partial}{\partial\beta}\varepsilon'\varepsilon$$

$$\Rightarrow\ -2X'Y+2X'X\hat{\beta}=0$$

$$\Rightarrow \; 2X'X\widehat{\beta} = 2X'Y$$

$$\Rightarrow \; \widehat{\beta} = (X'X)^{-1} X'Y \qquad 3.15$$

With the matrix, we can derive the β values for our regression analysis.

3.8 Geographic Information System (GIS) Data Processing

SBAS-InSAR results produced by Mintpy software is used to create GIS layers in ArcGIS®, and the velocity is interpreted as subsidence in the LOS direction. Results of Mintpy contain the information on latitude and longitude along with corresponding LOS velocity values time-series. Aside from that, the census data is also converted to GIS layers to proceed with OLS analysis using ArcGIS® software.

Chapter 4. Results

4.1 Visual Interpretation of InSAR Results

Figure 4.1 shows the surface displacement rate (mm/year) of the study area along LOS (Line of Sight) calculated over the generated interferograms for Dhaka city of Bangladesh.

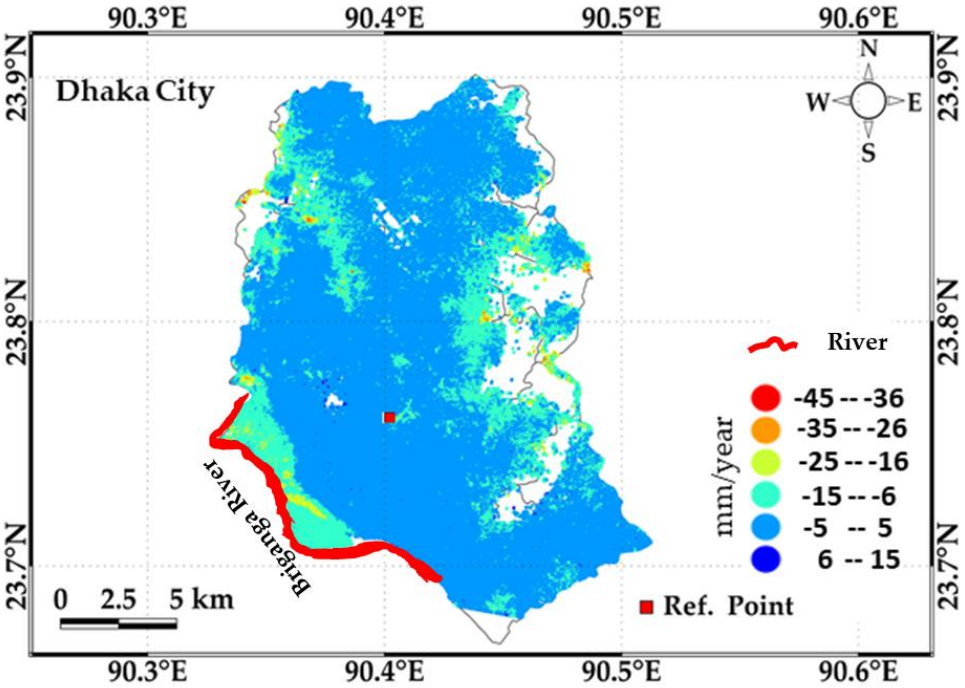

Figure 4.1 LOS velocity map of Dhaka City, Bangladesh.

Areas with large manmade structures showed a higher coherence. Mean velocity along the LOS direction for the study area has significant subsidence signals within Dhaka. A significant subsidence signal is being noticed in the southwestern part of the city. Also, the eastern part of the city exhibits subsidence signals, and the

northeastern part shows similar results. Most of the subsidence signals are coming from the areas along the rivers.

Figure 4.2 shows the study area's surface displacement rate (mm/year) along the LOS (Line of Sight) direction for Chittagong city of Bangladesh.

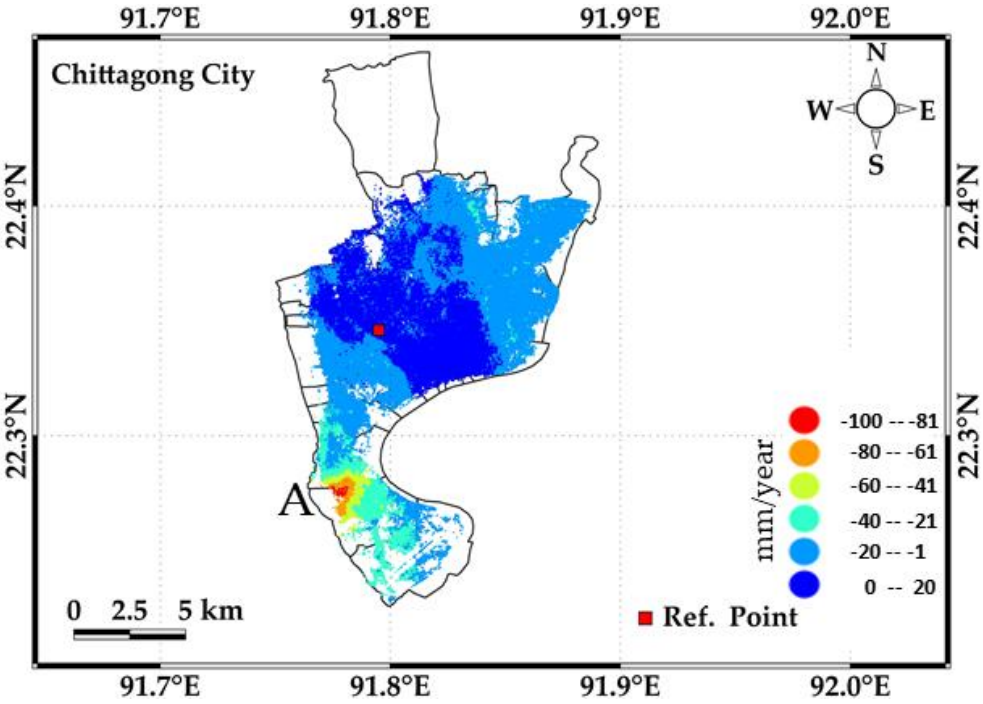

Figure 4.2 LOS velocity map of Chittagong City, Bangladesh.

Similarly like Dhaka city, Chittagong city also exhibits high coherence over manmade structures rather than the natural terrain. But for Chittagong city coastal area, close to the sea, shows a maximum amount of subsidence signal. It is worth noting that if the reference area is subsiding, genuine subsidence rates may be significantly higher in cities without publicly available GNSS data than what is calculated from InSAR data. The InSAR results of this study

can act as a guide for the placement of GNSS stations to monitor future subsidence. For the case of Chittagong city selection of the reference point is done by considering typically an elevated region away from the shore where the soil class is different from the subsiding region.

In this study, at first visual analysis is done on the ground subsidence over the urban areas of Bangladesh from InSAR results. From Figure 4.3, It is visible that in Dhaka city, subsidence dominates in the region with soil classes D3, D4, and D5 corresponding to soil class alluvial (Floodplain: sands, silt, and clays 6-15 m thick) [51]. Finally, the subsidence function coincides with the soil class to some extent. In Chittagong city, the subsidence signal is more evident in the region with soil class csd (beach and dune sand, coastal deposit).

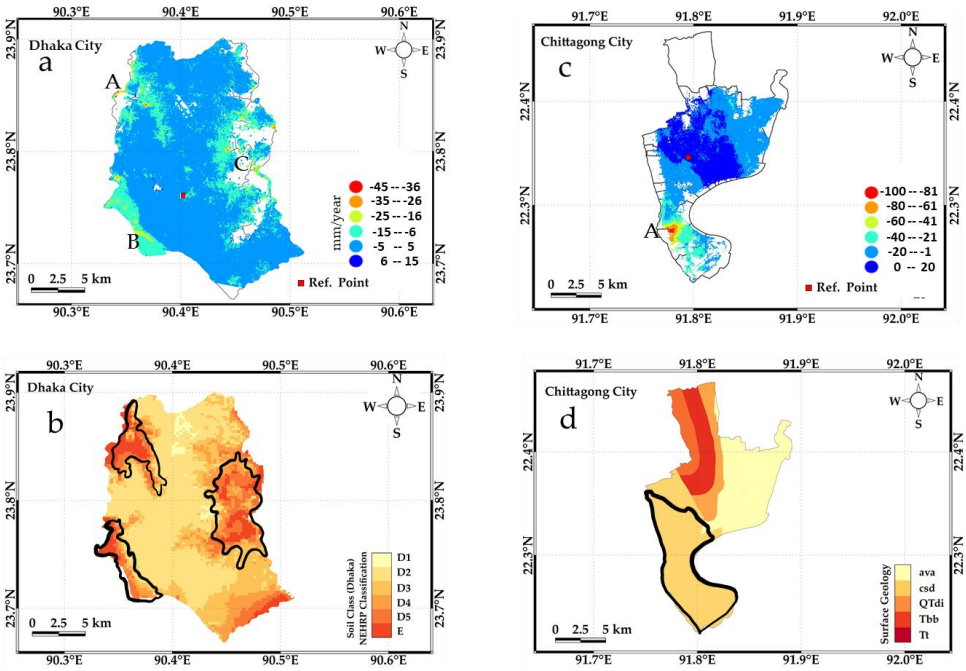

Figure 4.3 LOS velocity map of the study area and the soil class.

The Dhaka region is mostly composed of alluvium, which is a mix of silt, clay, and sand. The alluvium is divided into five classes based

on its grain-size distribution. Class D3, D4, and D5 are fine-grained alluvium, while classes D1 and D2 are coarse-grained alluvium. In general, the finer the alluvium, the greater the subsidence [52].

The Chittagong region is mostly composed of coastal deposits, which are unconsolidated materials such as sand, silt, and clay that the sea has deposited. The subsidence in this region is likely due to the consolidation of these materials over time. Land subsidence happens when water is withdrawn from fine-grained, highly compressible sediments, such as clay and silt interbeds in an aquifer [53].

4.2 Time-series of InSAR Results

Dhaka, the capital of Bangladesh, is one of the fastest-sinking cities in the world. Figure 4.4 shows the time series of LOS velocity for Dhaka, which reveals that the city is sinking at a maximum of 44 mm/year in the northwestern part, 25 mm/year in the southwestern part, and 37 mm/year in the eastern part in LOS direction. Significant subsiding part (Location: B, Kamrangir Char, Dhaka) showing average subsidence of about 12 mm/year in LOS the direction corresponds to soil class artificial landfills. This rapid subsidence of Dhaka is caused by a combination of natural and human factors. The city is built on the delta of the Ganges, Brahmaputra, and Meghna rivers, constantly depositing sediment. In addition, the extensive groundwater extraction by Dhaka's 10 million residents is causing the soil to compact and the land to sink. The central part of the city is much more stable in terms of subsidence.

The city of Chittagong in Bangladesh is facing an alarming rate of ground subsidence, with LOS rates reaching up to 90 mm/year. This is possibly due to the excessive extraction of groundwater from the aquifers beneath the city. The problem is compounded by the fact that the city is built on soft clay specifically the subsiding area, which is

especially vulnerable to subsidence. It is worth noting that even though Chittagong city is the second largest city in Bangladesh but it's not within the coverage of the Bengal Delta.

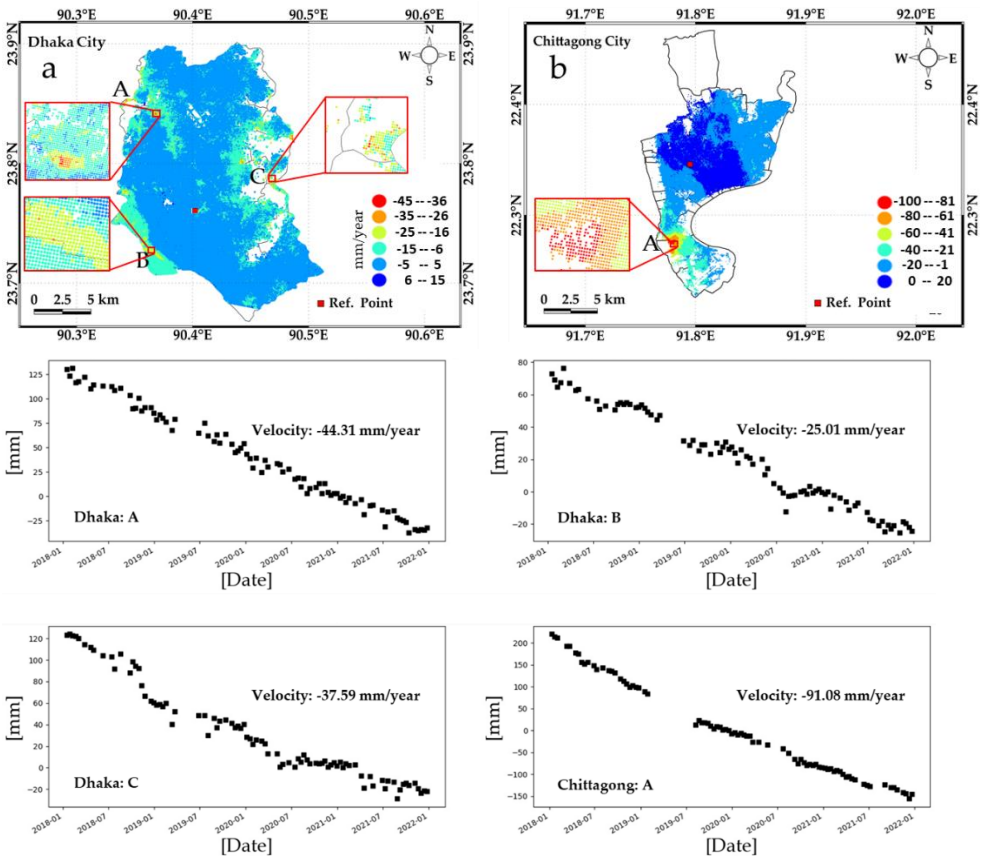

Figure 4.4 Displacement time series extracted for the points selected with the red square in area of interest Dhaka and Chittagong, Bangladesh.

Figure 4.6 and 4.7 shows Interferometric range change evolution over our study area during the study period.

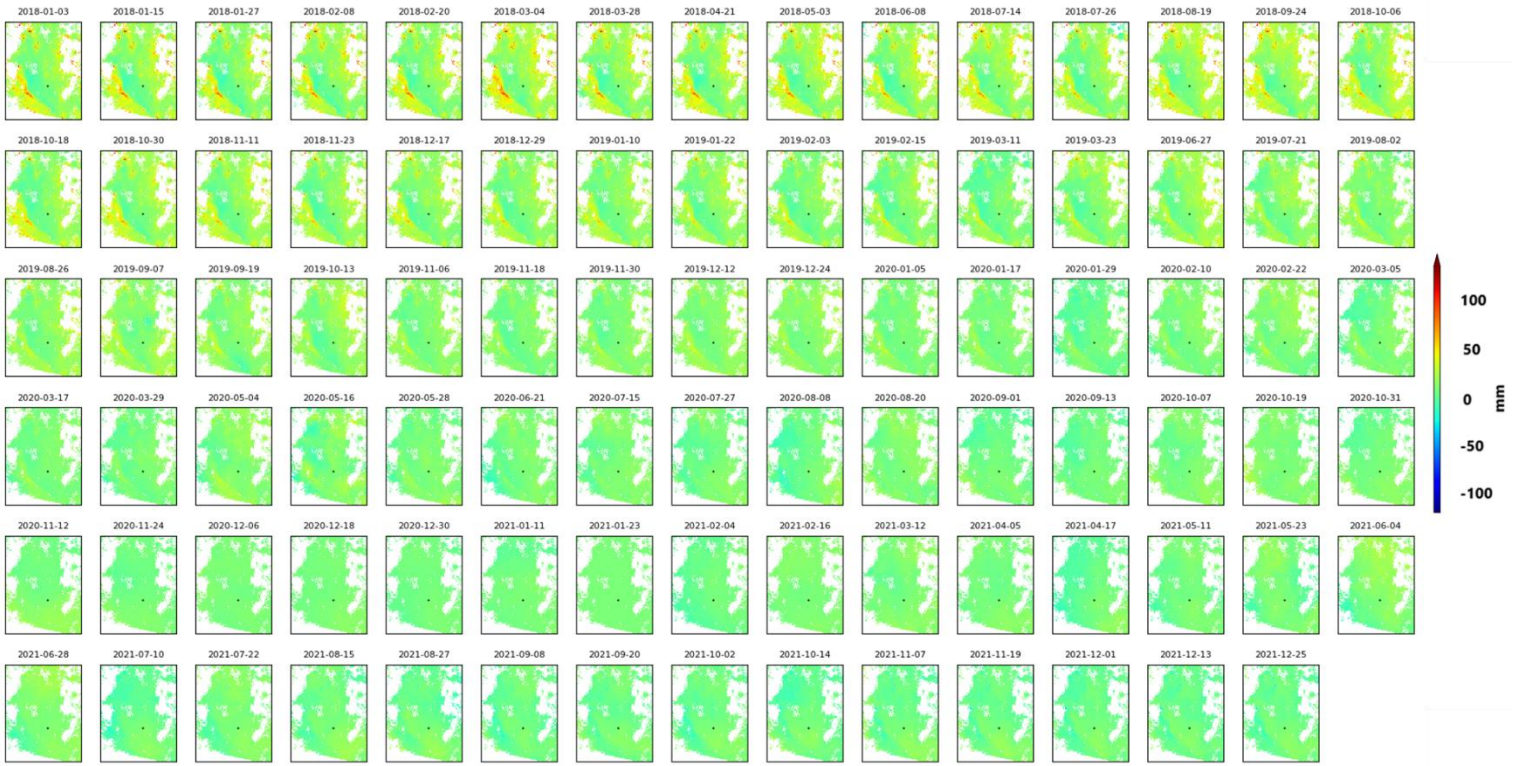

Figure 4.6 Interferometric range change evolution over Dhaka city, Bangladesh.

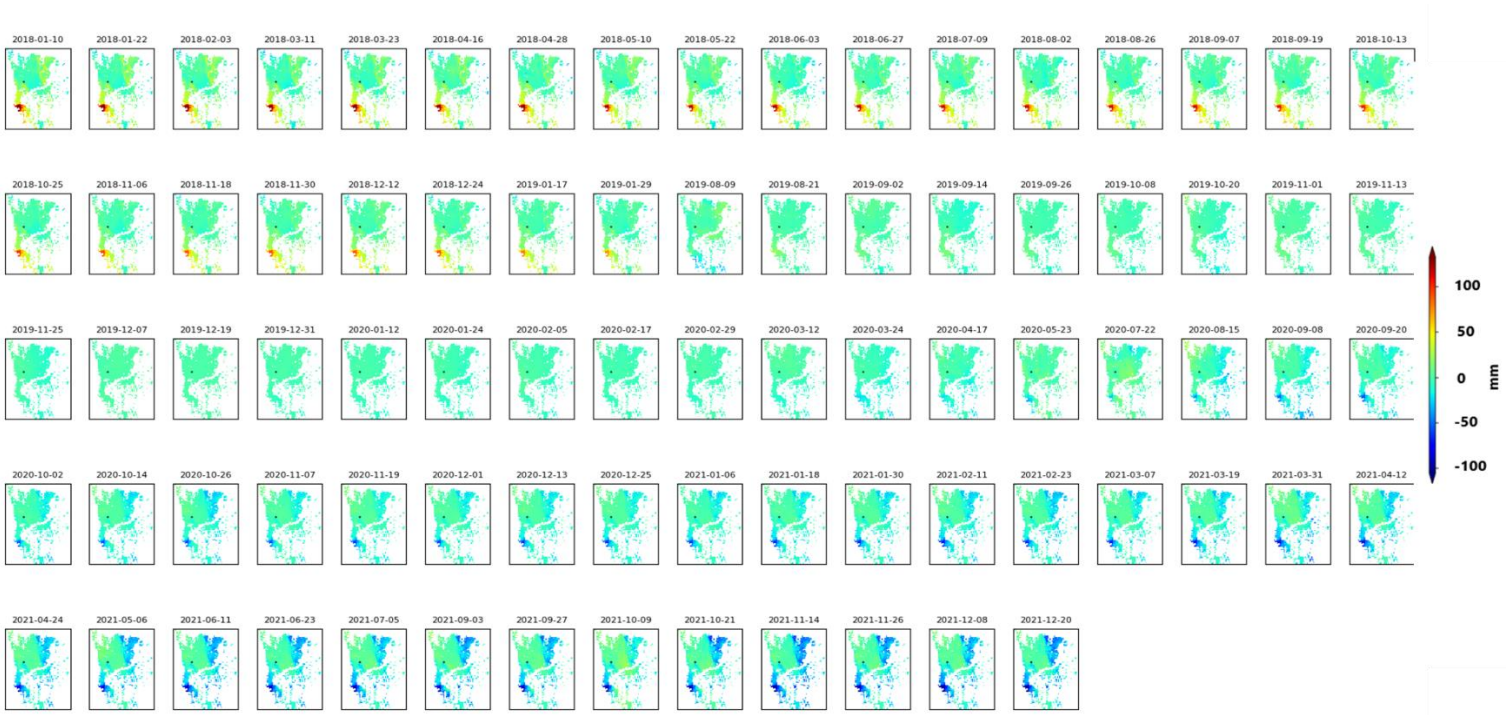

Figure 4.7 Interferometric range change evolution over Chittagong city, Bangladesh.

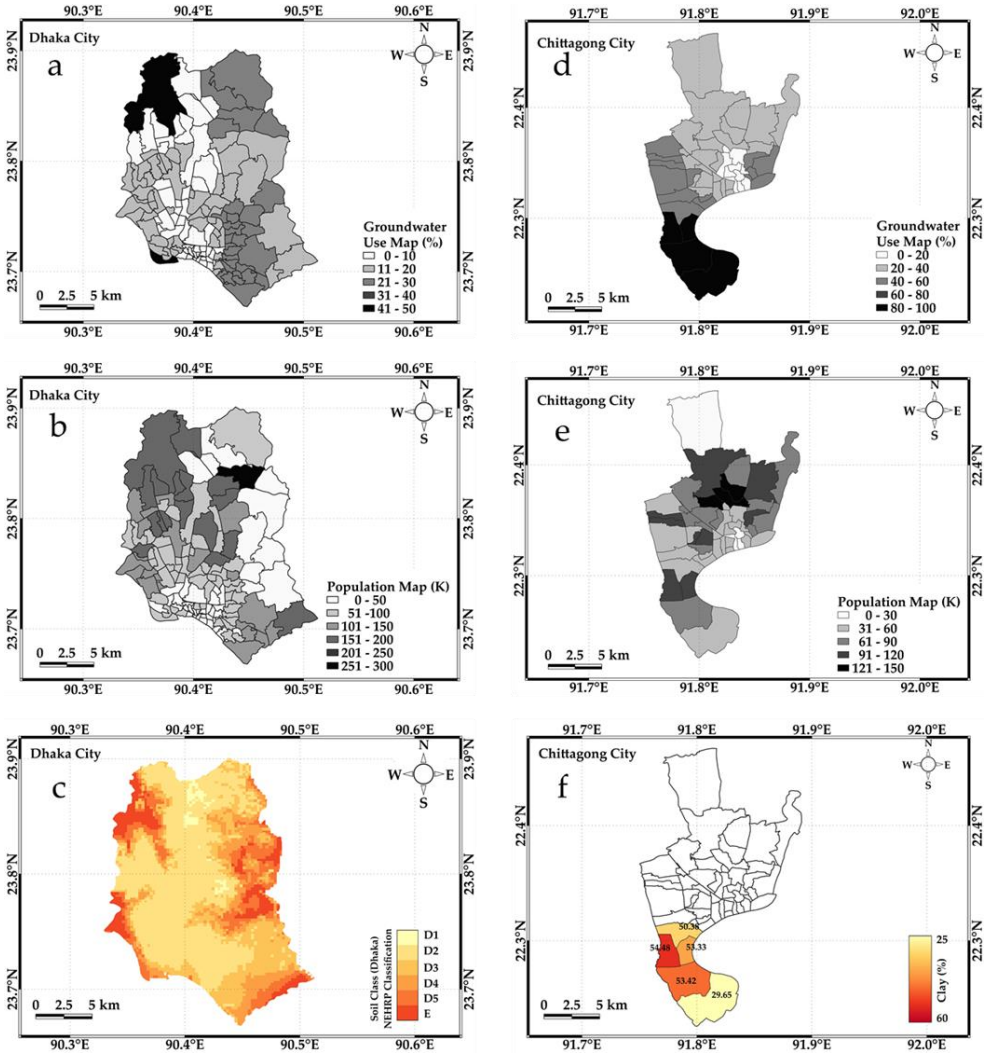

Figure 4.8 Groundwater use (%), population, soil class (Dhaka), and clay %, Chittagong [39]) map over major urban areas in Bangladesh [38].

Groundwater is often used as a resource for cities, but too much use can lead to subsidence. Excessive use of groundwater led to the failure of soil support for infrastructure. This can be a problem for buildings and infrastructure already existing on it. Figure 4.7 shows

different possible factors of land subsidence in Dhaka and Chittagong city. The factors do not show a clear relationship between groundwater use, population, soil class, and subsidence for Dhaka and Chittagong city. Many factors can contribute to subsidence, including natural causes. It is important to understand all of the factors involved in order to find the best solution.

When it comes to understanding the relationship between groundwater use, population, and soil class, it's much more a complex system. The standard methods of data collection and analysis don't always cut it when it comes to proving hypotheses in this area. To prove the hypothesis that there is a relationship between these three factors, initiatives taken for further analysis to find spatial relationships in the results. By analyzing it is possible to get a clearer picture of the relationships at their place. It is hoped that this research will shed light on this complex issue and help people to understand better the role that each of these factors plays in the overall situation.

4.3 Spatial Analysis of InSAR Results

To fully understand the implications of the factors causing subsidence, it is necessary to investigate the results. This process of estimation is capable of proving the contribution of different aspects to the subsidence that InSAR measures. To make an accurate estimation, I first needed to normalize the InSAR results. By doing this, finding the relationship among different factors is easier with the subsidence. To do so, U first estimated the statistics (Average, Max, Min) of each polygon (administrative units) for InSAR results. Therefore, execution of OLS estimation is done for the results.

4.3.1 OLS Analysis of the InSAR Results

From our OLS estimation, the R-squared value is 0.21 for Dhaka and 0.81 for Chittagong, respectively using both normalized and standardized data. Specifically for Dhaka, the OLS model shows a comparatively lower R-Squired value, which means that the average LOS speed can only be explained by about 21 percent. In comparison, for Chittagong city, the R-Squired value is quite significant, and the dependent variable is explained about 81 percent by the explanatory variables. Table 4.1 describes the result of our OLS analysis.

Table 4.1 OLS analysis results of InSAR results.

OLS Results Dhaka City	Summary of OLS Results (Dhaka City) Normalized Data	Summary of OLS Results (Dhaka City) Standardized Data
Variables	Coeff.	Coeff.
GW use	-0.26	-0.30
Population	0.02	0.03
Soil Class (M. Stiff)	-0.08	-0.41
Soil Class (L. Stiff)	-0.16	-0.82
Soil Class (A. Fill)	-0.21	-1.05
R2	0.21	0.21

OLS Results Chittagong City	Summary of OLS Results (Chittagong City) Normalized Data	Summary of OLS Results (Chittagong City) Standardized Data
Variables	Coeff.	Coeff.
GW use	-0.44	-0.48
Population	-0.16	-0.19
Clay	-0.38	-0.44
R2	0.81	0.81

N:B: S_Class (M. Stiff) = Moderate Stiff Soil, S_Class (L. Stiff) = Low Stiff Soil, S_Class (A. Fill) = Artificial Land Filling.

Chapter 5. Discussion

This study focused on the ground motion rate in the two largest urban areas of Bangladesh, Dhaka, and Chittagong, and significant subsidence (LOS direction) is observed in both Dhaka and Chittagong. The average LOS velocity in the city of Dhaka is estimated to be around 12 mm/year in the southern part of Dhaka city, which is similar to the 11.2 mm/year found in a previous study [35]. A possible reason for the difference in measurements by [11], could be due to the method. Which measured average subsidence of 3.8 mm/year, while measurements from GPS showed subsidence of about 12.4 mm/year [35]. In Chittagong city, LOS velocity measured about 90 mm/year. It is also noticeable that the city's subsidence is much more on a local basis.

The subsidence in Chittagong is much more complex rather than the Dhaka city. The subsidence in Chittagong city is highly dominated by a single sub-surface soil class which is a coastal deposit (beach and dune sand). So to find the relationship with the geological setting, an Investigation of the soil strata shows that subsidence in this area is much more related to the clay proportion. The re-alignment (compaction) of fine-grained minerals such as clay, results in the permanent loss of pore space. The water content in sediment is related to the clay content; as a result, clay-rich sediments will lose more water than sandy ones. This results in the sinking of landmass, especially for soils with high concentrations of clay [54].

The subsidence measurements presented with this study using the SBAS-InSAR method exhibit a relationship to the soil class, groundwater use, and population. If we concentrate on OLS analysis results, we see that both the major urban area of Bangladesh shows significant relation with the average velocity of corresponding

administrative units, especially geological setting. It is worth highlighting that, the OLS model over both the study area is explaining the variability of average LOS velocity in terms of global extent.

The results of this study are based on the data corresponding to the polygon area. However, since this is not specific spatial information, there may be some anomalies. This is a limitation of the study that should be taken into consideration. I didn't have the groundwater pumping data available when I took the subsidence measurements. It's difficult to make a definitive determination about the subsidence without that data. Without the data, it's hard to say for certain whether or not the subsidence is due to groundwater pumping. However, It can be believed that the subsidence is likely due to groundwater pumping, and surface geology based on the spatial relationship shown in the OLS results. In the Chittagong area, I found that the data is not highly coherent. This could cause some anomalies in the results. I also found that some of the data is missing from February to September 2019 (was not available), which could again cause some problems with the time-series results.

The potential groundwater recharge rate for Dhaka city is 1.33 m/y, but the groundwater depletion rate is 2.81 m/y. As a result, despite enough rainfall, Dhaka city faces a 1.48 m/y groundwater recharge deficit every year. The problem will deteriorate as the rate of urbanization accelerates and surface water bodies diminish [55]. Even though for Dhaka city, the correlation did not show a significant association with subsidence. One possible reason behind this may be the undocumented uses of groundwater.

The derived results with this study, use data (groundwater use, population, and soil class) for the corresponding polygon area which is not the specific spatial information, as a result, there may have some anomalies which is a limitation of this study. At the same time, data unavailability of groundwater pumping correlates with the subsidence

estimated using the InSAR technique. For the Chittagong area, I have noticed that coherence (Figure 6) is not high which may cause some anomalies in the results too.

Chapter 6. Conclusion

The study's overall objective is to conduct a time series analysis to determine the subsidence pattern in Dhaka and Chittagong between 2018 and 2021. Over time, the time series analysis (SBAS-InSAR) shows that the land is subsiding faster in parts along the major urban areas of Bangladesh. This global problem is primarily due to local human activities in each city, especially groundwater extraction. The most rapid land subsidence occurs in the southwest, northwest, and east of Dhaka city, where population and groundwater use are also higher. In addition, the geological nature of Dhaka is also responsible for subsidence to the most extent found in this study. Dhaka's surface subsidence shown seasonal fluctuations with rainfall. Furthermore, the rains efficiently replenished the soil water content and groundwater level. The summer season and lack of rain boosted water use as well as the rate of soil subsidence.A similar trend in terms of geology observed in the city of Chittagong. The strongest subsidence signals come from the areas with residential and industrial areas and the most groundwater use at the same time the clay proportion in subsiding areas is also higher. This indicates that subsidence in urban areas of Bangladesh is caused by groundwater extraction and geological conditions. The highest LOS velocity is estimated at 44 mm/year with an average of about 12 mm/year at most subsiding areas in Dhaka and 90 mm/year (highest) in Chittagong. Our results show that the OLS analysis is capable of explaining the average LOS velocity variability of about 21 and 81 percent respectively both with normalized and standardized datasets. The findings of this study could help Bangladesh better prepare for and manage the impacts of subsidence. In addition, the findings of this study may also be helpful to other countries facing similar risks from subsidence. At the same time, the

subsidence of Chittagong city is alarming and continuous monitoring of this area is necessary for further study.

References

1. Miall, A.D., *Facies Models 4. Deltas.* Geoscience Canada, 1976. **3**(3).

2. Giosan, L., et al., *Climate change: Protect the world's deltas.* Nature, 2014. **516**(7529): p. 31-33.

3. Woodroffe, C., et al., *Global change and integrated coastal management: the Asia-Pacific region, coastal systems and continental margins.* 2006.

4. Syvitski, J.P., et al., *Sinking deltas due to human activities.* Nature Geoscience, 2009. **2**(10): p. 681-686.

5. Huang, B., L. Shu, and Y. Yang, *Groundwater overexploitation causing land subsidence: hazard risk assessment using field observation and spatial modelling.* Water resources management, 2012. **26**(14): p. 4225-4239.

6. Crossland, C.J., et al., *Coastal fluxes in the Anthropocene: the land-ocean interactions in the coastal zone project of the International Geosphere-Biosphere Programme*. 2005: Springer Science & Business Media.

7. Nicholls, R.J., et al., *Coastal systems and low-lying areas.* 2007.

8. Cao, A., et al., *Future of Asian Deltaic Megacities under sea level rise and land subsidence: current adaptation pathways for Tokyo, Jakarta, Manila, and Ho Chi Minh City.* Current Opinion in Environmental Sustainability, 2021. **50**: p. 87-97.

9. Akter, J., et al., *Evolution of the Bengal Delta and its prevailing processes.* Journal of Coastal Research, 2016. **32**(5): p. 1212-1226.

10. Brown, S. and R. Nicholls, *Subsidence and human influences in mega deltas: the case of the Ganges–Brahmaputra–Meghna.* Science of the Total Environment, 2015. **527**: p. 362-374.

11. Higgins, S.A., et al., *InSAR measurements of compaction and subsidence in the Ganges-Brahmaputra Delta, Bangladesh.* Journal of Geophysical Research: Earth Surface, 2014. **119**(8): p. 1768-1781.

12. Du, Z., et al., *Correlating the subsidence pattern and land use in Bandung, Indonesia with both Sentinel-1/2 and ALOS-2 satellite images.* International journal of applied earth observation and geoinformation, 2018. **67**: p. 54-68.

13. Rosi, A., et al., *Subsidence mapping at regional scale using persistent scatters interferometry (PSI): The case of Tuscany region (Italy).* International journal of applied earth observation and geoinformation, 2016. **52**: p. 328-337.

14. Peduto, D., et al., *A general framework and related procedures for multiscale analyses of DInSAR data in subsiding urban areas.* ISPRS journal of photogrammetry and remote sensing, 2015. **105**: p. 186-210.

15. Castellazzi, P., et al., *InSAR to support sustainable urbanization over compacting aquifers: The case of Toluca Valley, Mexico.* International journal of applied earth observation and geoinformation, 2017. **63**: p. 33-44.

16. Zhang, Y., et al., *Characterization of land subsidence induced by groundwater withdrawals in the plain of Beijing city, China.* Hydrogeology Journal, 2014. **22**(2): p. 397-409.

17. Zhang, Q., et al., *Two-dimensional deformation monitoring over Qingxu (China) by integrating C-, L-and X-bands SAR images.* Remote Sensing Letters, 2014. **5**(1): p. 27-36.

18. Ortega-Guerrero, A., D.L. Rudolph, and J.A. Cherry, *Analysis of long-term land subsidence near Mexico City: Field investigations and predictive modeling.* Water resources research, 1999. **35**(11): p. 3327-3341.

19. Chatterjee, R.S., et al., *Subsidence of Kolkata (Calcutta) City, India during the 1990s as observed from space by Differential Synthetic Aperture Radar Interferometry (D-InSAR) technique.* Remote Sensing of Environment, 2006. **102**(1): p. 176-185.

20. Phien-wej, N., P.H. Giao, and P. Nutalaya, *Land subsidence in bangkok, Thailand.* Engineering geology, 2006. **82**(4): p. 187-201.

21. Osmanoğlu, B., et al., *Mexico City subsidence observed with persistent scatterer InSAR.* International Journal of Applied Earth Observation and Geoinformation, 2011. **13**(1): p. 1-12.

22. Ng, A.H.-M., et al., *Mapping land subsidence in Jakarta, Indonesia using persistent scatterer interferometry (PSI) technique with ALOS PALSAR.* International Journal of Applied Earth Observation and Geoinformation, 2012. **18**: p. 232-242.

23. Hoque, M. and M. Alam, *Subsidence in the lower deltaic areas of Bangladesh.* Marine Geodesy, 1997. **20**(1): p. 105-120.

24. Goodbred Jr, S. and S.A. Kuehl, *The significance of large sediment supply, active tectonism, and eustasy on margin sequence development: Late Quaternary stratigraphy and evolution of the Ganges–Brahmaputra delta.* Sedimentary Geology, 2000. **133**(3-4): p. 227-248.

25. Becker, M., et al., *Water level changes, subsidence, and sea level rise in the Ganges–Brahmaputra–Meghna delta.* Proceedings of the National Academy of Sciences, 2020. **117**(4): p. 1867-1876.

26. Ostanciaux, E., et al., *Present-day trends of vertical ground motion along the coast lines.* Earth-Science Reviews, 2012. **110**(1-4): p. 74-92.

27. Steckler, M.S., et al., *Synthesis of the distribution of subsidence of the lower Ganges-Brahmaputra Delta, Bangladesh.* Earth-Science Reviews, 2022. **224**: p. 103887.

28. Steckler, M.S., et al., *GPS Velocity Field in Bangladesh: Delta Subsidence, Seasonal Water Loading and Shortening Across the Burma Accretionary Prism and Shillong Massif*. 2013. p. T13D-2566.

29. Amelung, F., et al., *Sensing the ups and downs of Las Vegas: InSAR reveals structural control of land subsidence and aquifer-system deformation.* Geology, 1999. **27**(6): p. 483-486.

30. Hung, W.-C., et al., *Monitoring severe aquifer-system compaction and land subsidence in Taiwan using multiple sensors: Yunlin, the southern Choushui River Alluvial Fan.* Environmental Earth Sciences, 2010. **59**(7): p. 1535-1548.

31. Bell, J.W., et al., *Permanent scatterer InSAR reveals seasonal and long-term aquifer-system response to groundwater pumping and artificial recharge.* Water Resources Research, 2008. **44**(2).

32. Chang, C.P., et al., *Land-surface deformation corresponding to seasonal ground-water fluctuation, determining by SAR interferometry in the SW Taiwan.* Mathematics and Computers in Simulation, 2004. **67**(4): p. 351-359.

33. Casu, F., M. Manzo, and R. Lanari, *A quantitative assessment of the SBAS algorithm performance for surface deformation retrieval from DInSAR data.* Remote Sensing of Environment, 2006. **102**(3-4): p. 195-210.

34. Ferretti, A., et al., *Submillimeter accuracy of InSAR time series: Experimental validation.* IEEE Transactions on Geoscience and Remote Sensing, 2007. **45**(5): p. 1142-1153.

35. Haque, D.M.E. and T. Hayat, *TIME SERIES ANALYSIS OF SUBSIDENCE IN DHAKA CITY, BANGLADESH USING INSAR.* 2019. **3**: p. 32-44.

36. Rahman, M. and S. Quayyum, *Sustainable Water Supply In Dhaka City: Present And Future*. 2008.

37. Monsur, M., *Stratigraphical and palaeomagnetical studies of some quaternary deposits of the Bengal Basin, Bangladesh.* Unpublished D. Sc. Thesis, Vrije University. Brussels, Belgium, 1990: p. 241.

38. Statistics, B.B.o., *Population and Housing Census-2011*, M.o. Planning, Editor. 2011, Bangladesh Bureau of Statistics: Dhaka, Bangladesh. p. 657.

39. Zahid, A., K. Jahan, and K. Islam, *Feasibility Study for Multilane Road Tunnel under the River Karnaphuli, Chittagong, Bangladesh: REPORT ON GEOLOGICAL AND GEOTECHNICAL INVESTIGATION by DevCon, Bangladesh*. 2015.

40. Galloway, D., D.R. Jones, and S. Ingebritsen, *Land Subsidence in the United States.* U.S. Geological Survey Circular, 1999. **USGS Circ. 1182**.

41. Curlander, J.C. and R.N. Mcdonough. *Synthetic Aperture Radar: Systems and Signal Processing*. 1991.

42. Marghany, M., *Chapter 3 - Theories of microwave synthetic aperture radar*, in *Advanced Algorithms for Mineral and Hydrocarbon Exploration Using Synthetic Aperture Radar*, M. Marghany, Editor. 2022, Elsevier. p. 81-111.

43. Kim, S.Y. and N.-H. Myung, *An optimal antenna pattern synthesis for active phased array sar based on particle swarm optimization and adaptive weighting factor.* Progress In Electromagnetics Research C, 2009. **10**.

44. Massonnet, D. and K. Feigl, *Massonnet, D. & Feigl, K. L. Radar interferometry and its application to changes in the Earth's surface. Rev. Geophys. 36, 441-500.* Reviews of Geophysics, 1998. **36**.

45. Zebker, H.A. and J. Villasenor, *Decorrelation in interferometric radar echoes.* IEEE Transactions on geoscience and remote sensing, 1992. **30**(5): p. 950-959.

46. Hanssen, R., *Radar Interferometry Data Interpretation and Error Analysis*. Vol. 2. 2001.

47. Ferretti, A., C. Prati, and F. Rocca, *Permanent scatterers in SAR*

interferometry. IEEE Transactions on Geoscience and Remote Sensing, 2001. **39**(1): p. 8-20.

48. Berardino, P., et al., *A new algorithm for surface deformation monitoring based on small baseline differential SAR interferograms.* IEEE Transactions on Geoscience and Remote Sensing, 2002. **40**(11): p. 2375-2383.

49. Yunjun, Z., H. Fattahi, and F. Amelung, *Small baseline InSAR time series analysis: Unwrapping error correction and noise reduction.* Computers & Geosciences, 2019. **133**: p. 104331.

50. Zdaniuk, B., *Ordinary Least-Squares (OLS) Model*, in *Encyclopedia of Quality of Life and Well-Being Research*, A.C. Michalos, Editor. 2014, Springer Netherlands: Dordrecht. p. 4515-4517.

51. Hoque, M.A., M.M. Hoque, and K.M. Ahmed, *Declining groundwater level and aquifer dewatering in Dhaka metropolitan area, Bangladesh: causes and quantification.* Hydrogeology Journal, 2007. **15**(8): p. 1523-1534.

52. salehi moteahed, F., et al., *Geological parameters affected land subsidence in Mashhad plain, north-east of Iran.* Environmental Earth Sciences, 2019. **78**.

53. Hoffmann, J., et al., *MODFLOW-2000 Ground-Water Model—User guide to the subsidence and aquifer-system compaction (SUB) package.* USGS Ground-Water Resour. Program Open-File Rep., 2003: p. 55.

54. W. A Segeren, H.S., *DRAINAGE PRINCIPLES AND APPLICATIONS: Drainage of newly reclaimed marine clayey sediments, peat soils, and acid sulphate soils*. 1980, 16 Wageningen: ILRI Publication. 261-295.

55. Uddin A.F.M Azim & Baten, M.A., *WATER SUPPLY OF DHAKA CITY: MURKY FUTURE THE ISSUE OF ACCESS AND INEQUALITY*. 2011, Unnayan Onneshan-The Innovators.

Abstract

이 논문은 방글라데시 주요 도시 지역의 지반 침하를 측정하는 것을 목표로 한다. 지반 침하는 자연 요인(상승하는 물, 퇴적물 압축, 지각 구조 및 퇴적물 공급 감소) 또는 인위적 요인(유체 추출)으로 인해 발생하며, 이러한 현상은 Nagoya(일본), Venice(이탈리아), San Joaquin Valley 및 Long Beach(미국 캘리포니아), Houston(미국 텍사스) 등 전 세계 도시 지역에 대해 영향을 미치고 있다. 마찬가지로 기존 선행연구에서 방글라데시의 Dhaka와 Chittagong의 침하가 입증되었으나 관측된 침하 속도가 서로 상이하기에 침하의 원인이나 기작이 정밀하게 연구되지 않았다.

위성 기반 방법인 InSAR (Interferometric Synthetic Aperture Radar)는 mm 단위의 정확도로 광대한 지역에 걸쳐 지면 변형을 도시하는 데 효과적이다. InSAR 기법을 활용한 지반 변위 정량은 다른 연구 기법들과 복합적으로 활용할 경우 지반 변위 및 운동의 원인과 기작을 정밀하게 조사하여 침하의 원인에 대한 중요한 정보를 제공할 수 있기에, 이에 본 연구에서는 SBAS-InSAR 기술, 지하수 사용에 대한 인구 조사 보고서, 토양 분류도와 함께 인구를 결합하여 해당 매개변수와의 공간적 관계를 조사하였다. 본 연구는 2018년 1월부터 2021년 12월까지 방글라데시에 위치한 Chittagong과 Dhaka에서의 지반 운동의 시공간적 특성을 분석하였다.

Small Baseline Subset 알고리즘은 공간 비상관성 문제를 최소화하기 위해 적용되는 기술로, Sentinel-1 SAR 위성 데이터를 기반으로 LOS(시선) 속도를 계측하는데 사용되었다. InSAR 기법을 사용한 변위 정량 결과는 Dhaka와 Chittagong의 일부 지역에서 LOS 방향을 따라 상당한 속도로침하가 발생하고 있음을 보여주었다. 측정된 LOS 속도의 관측폭은 두 연구 지역에 걸쳐공간적으로 다양하게 관측되었다. 침하 양상은 지질학적 환경 및 지하수 사용과 밀접한 관련이 있으며, 이를 통해 방글라데시의 주요 도시 지역에 대한 최근의 지반 침하 가능성과 속도를 추정할 수 있었습니다. 이 연구는 또한 GPS

자료, 지반 조사 등과 같은 지속적인 관찰 기술을 사용하여 방글라데시의 도시 지역을 모니터링할 것을 제안하였다. 또한, 본 연구에서 관측한 Chittagong 지역의 큰 지반 변위 관측치에 기반하여, 해당 지역의 전역적인 지반 조사를 제안하였다.

Keywords: SBAS-InSAR, 침하, Dhaka, Chittagong, 시계열 분석
학번: 2020-22032

Appendix

Appendix 1: Groundwater use and population data from Population and Housing Census Report 2011, and soil texture from NEHRP soil class, Dhaka City:

SL No.	Ward Name	City	Groundwater Use (%)	Popu (K)	Soil Texture Class
1	Badda	Dhaka	18	180.6	D2
2	Beraid	Dhaka	18	14.9	D4
3	Bhatara	Dhaka	18	126.7	D5
4	Dakshingaon (Part)	Dhaka	29	37.2	D4
5	Dakshingaon (Part)	Dhaka	21.1	33.0	D2
6	Dakshinkhan (part)	Dhaka	7.6	5.5	D2
7	Dakshinkhan (part)	Dhaka	24.1	255.9	D4
8	Dakshinkhan (Part)	Dhaka	21.3	11.4	D2
9	Demra (part)	Dhaka	19.4	35.8	D4
10	Dhania (part)	Dhaka	23.5	122.2	D3
11	Dhania (part)	Dhaka	20.4	122.2	D3
12	Dumni	Dhaka	24.1	16.9	E
13	Harirampur (Part)	Dhaka	42.7	157.3	D3
14	Manda	Dhaka	21.1	62.3	D2
15	Matuail (part)	Dhaka	19.4	136.9	D4
16	Matuail (part)	Dhaka	23.5	136.9	D2
17	Matuail (part)	Dhaka	20.4	136.9	D4
18	Nasirabad	Dhaka	29	0.0	E
19	Saralia	Dhaka	19.4	156.6	Water
20	Satarkul	Dhaka	18	23.7	D4
21	Shyampur	Dhaka	20.4	117.0	D3
22	Sultanganj	Dhaka	44.1	93.6	D5
23	Uttar Khan	Dhaka	25.1	78.9	D2

24	Ward No-01	Dhaka	7.6	183.3	D2
25	Ward No-01	Dhaka	3.1	183.3	D3
26	Ward No-02	Dhaka	4	151.9	E
27	Ward No-03	Dhaka	4	94.7	D5
28	Ward No-04	Dhaka	18.2	75.2	D4
29	Ward No-05	Dhaka	4	118.1	D5
30	Ward No-06	Dhaka	4	163.8	E
31	Ward No-07 (Part)	Dhaka	10.3	113.8	D2
32	Ward No-08	Dhaka	9.8	111.3	E
33	Ward No-09	Dhaka	12	71.3	D2
34	Ward No-10	Dhaka	12	87.9	D2
35	Ward No-11	Dhaka	10.3	97.0	D2
36	Ward No-12	Dhaka	10.3	116.5	D2
37	Ward No-13	Dhaka	10.3	157.2	D2
38	Ward No-14 (part)	Dhaka	18.2	163.8	D2
39	Ward No-14 (part)	Dhaka	10.3	163.8	D2
40	Ward No-15 (part)	Dhaka	1.3	173.8	D2
41	Ward No-15 (part)	Dhaka	18.2	173.8	D2
42	Ward No-15 (part)	Dhaka	4	173.8	D2
43	Ward No-16	Dhaka	18.2	142.4	D2
44	Ward No-17 (Part)	Dhaka	18	196.5	D4
45	Ward No-17 (Part)	Dhaka	24.1	196.5	D4
46	Ward No-18	Dhaka	5	63.6	D1
47	Ward No-19	Dhaka	5	159.9	D2
48	Ward No-20 (Part)	Dhaka	5	98.6	D2
49	Ward No-20 (Part)	Dhaka	19.6	98.6	D2
50	Ward No-21	Dhaka	18	96.1	D2
51	Ward No-22	Dhaka	18.9	160.3	D3
52	Ward No-23	Dhaka	18.9	63.8	D3
53	Ward No-24	Dhaka	29	68.9	D3
54	Ward No-25	Dhaka	29	113.3	D5
55	Ward No-26	Dhaka	29	86.9	D5
56	Ward No-27	Dhaka	21.1	82.7	D3
57	Ward No-28	Dhaka	21.1	60.8	D3
58	Ward No-29	Dhaka	21.1	79.3	D2

59	Ward No-30	Dhaka	21.1	58.3	D2
60	Ward No-31	Dhaka	10.7	34.9	D2
61	Ward No-32	Dhaka	10.7	42.1	D2
62	Ward No-33	Dhaka	10.7	22.0	D2
63	Ward No-34	Dhaka	10.7	60.0	D2
64	Ward No-35	Dhaka	10.7	51.1	D2
65	Ward No-36	Dhaka	1.1	59.6	D2
66	Ward No-37	Dhaka	19.6	103.3	D3
67	Ward No-38 (Part)	Dhaka	9.5	99.7	D2
68	Ward No-38 (Part)	Dhaka	19.6	99.7	D2
69	Ward No-39	Dhaka	9.5	67.9	D2
70	Ward No-40 (Part)	Dhaka	8.9	90.2	D2
71	Ward No-40 (Part)	Dhaka	9.5	90.2	D2
72	Ward No-41	Dhaka	8.9	66.0	D3
73	Ward No-42	Dhaka	13.7	54.7	D2
74	Ward No-43	Dhaka	16.7	186.6	D2
75	Ward No-44	Dhaka	13.7	51.4	D2
76	Ward No-45	Dhaka	13.7	73.0	D2
77	Ward No-46	Dhaka	16.7	114.8	D5
78	Ward No-46	Dhaka	13.7	114.8	E
79	Ward No-46 (Part)	Dhaka	15.8	114.8	D4
80	Ward No-47 (part)	Dhaka	13.7	106.5	D2
81	Ward No-47 (Part)	Dhaka	5.6	106.5	D2
82	Ward No-48 (Part)	Dhaka	5.6	128.9	D2
83	Ward No-48 (Part)	Dhaka	15.8	128.9	D2
84	Ward No-49	Dhaka	5.6	72.4	D2
85	Ward No-50	Dhaka	2.7	80.0	D2
86	Ward No-51 (part)	Dhaka	13.7	58.9	D2
87	Ward No-51 (Part)	Dhaka	2.7	58.9	D2
88	Ward No-52	Dhaka	0.7	49.5	D2
89	Ward No-53	Dhaka	15.3	55.9	D2
90	Ward No-54	Dhaka	15.3	74.1	D4
91	Ward No-55	Dhaka	15.3	71.0	D2
92	Ward No-56 (part)	Dhaka	3.5	38.2	D2
93	Ward No-56 (Part)	Dhaka	18.7	38.2	D2

94	Ward No-57	Dhaka	3.5	33.5	D2
95	Ward No-58	Dhaka	15.8	88.5	D3
96	Ward No-59	Dhaka	18.7	48.9	D2
97	Ward No-60	Dhaka	18.7	66.5	D2
98	Ward No-61	Dhaka	18.7	29.8	D2
99	Ward No-62	Dhaka	18.7	44.5	D2
100	Ward No-63 (Part)	Dhaka	4	28.5	D3
101	Ward No-63 (Part)	Dhaka	5.5	28.5	D3
102	Ward No-64	Dhaka	5.5	24.7	D2
103	Ward No-65		5.5	58.2	D3
104	Ward No-66 (Part)	Dhaka	4	33.6	D3
105	Ward No-66 (Part)	Dhaka	5.5	33.6	D3
106	Ward No-67 (part)	Dhaka	4	35.7	D3
107	Ward No-67 (Part)	Dhaka	5.5	35.7	D2
108	Ward No-68 (part)	Dhaka	4	36.1	D3
109	Ward No-68 (Part)	Dhaka	4.2	36.1	D3
110	Ward No-69	Dhaka	4	65.3	D2
111	Ward No-70	Dhaka	4	50.6	D2
112	Ward No-71 (Part)	Dhaka	4	28.1	D2
113	Ward No-71 (Part)	Dhaka	4.2	28.1	D3
114	Ward No-72	Dhaka	4.2	26.2	D3
115	Ward No-73	Dhaka	4.2	18.2	D3
116	Ward No-74	Dhaka	6.7	46.1	D2
117	Ward No-75	Dhaka	6.7	38.3	D2
118	Ward No-76 (Part)	Dhaka	10.7	46.4	D2
119	Ward No-76 (Part)	Dhaka	23.5	46.4	D2
120	Ward No-77	Dhaka	6.7	40.6	D2
121	Ward No-78	Dhaka	6.7	27.9	D2
122	Ward No-79	Dhaka	6.7	40.0	D2
123	Ward No-80 (Part)	Dhaka	10.7	26.9	D2
124	Ward No-80 (Part)	Dhaka	6.7	26.9	D2
125	Ward No-81	Dhaka	10.7	50.4	D2
126	Ward No-82	Dhaka	10.7	40.3	D2
127	Ward No-83	Dhaka	24.3	48.0	D3
128	Ward No-84	Dhaka	23.5	58.7	D2

129	Ward No-85	Dhaka	23.5	61.0	D2
130	Ward No-86	Dhaka	23.5	56.8	D3
131	Ward No-87	Dhaka	24.3	69.4	D2
132	Ward No-88	Dhaka	20.4	44.0	D3
133	Ward No-89	Dhaka	20.4	59.0	D3
134	Ward No-90	Dhaka	24.3	66.6	D3
135	Ward No-91	Dhaka	18.7	22.4	D4
136	Ward No-92	Dhaka	18.7	82.1	D3
137	Ward No-98 (Part)	Dhaka	7.6	1.7	D2
138	Ward No-98 (Part)	Dhaka	1.3	61.2	D2

N:B: Popu is the short form of Population.

Appendix 2: Groundwater use and population data from Population and Census Report 2011, and clay (%) are from analyzing the soil profile data, Chittagong City:

SL No.	Ward Name	City	Groundwater Use (%)	Popu. (Thus.)	Clay (%)
1	Ward No-17	CHTT	2.2	97	
2	Ward No-18	CHTT	4.7	66	
3	Ward No-19	CHTT	0.9	76	
4	Ward No-35 (part1)	CHTT	2.7	31	
5	Ward No-01	CHTT	27.1	29	
6	Ward No-02	CHTT	16.9	103	
7	Ward No-03	CHTT	6.5	69	
8	Ward No-04	CHTT	11.3	108	
9	Ward No-05	CHTT	9.9	86	
10	Ward No-06	CHTT	2.8	62	
11	Ward No-36 (Par1)	CHTT	1.6	44	
12	Ward No-37	CHTT	4.4	42	
13	Ward No-38	CHTT	5.9	60	50.38
14	Ward No-39 (Part1)	CHTT	3.8	106	53.33
15	Ward No-12 (Part1)	CHTT	0.9	74	
16	Ward No-23	CHTT	0.7	31	
17	Ward No-24 (part1)	CHTT	2.4	109	
18	Ward No-27	CHTT	1.7	67	
19	Ward No-28	CHTT	1.7	50	
20	Ward No-29	CHTT	0.9	44	
21	Ward No-30 (Part1)	CHTT	0.4	46	
22	Ward No-36 (Part)	CHTT	0.7	44	
23	Ward No-11 (Part1)	CHTT	2.3	94	
24	Ward No-24 (part)	CHTT	0.7	109	
25	Ward No-25	CHTT	1.8	50	
26	Ward No-26	CHTT	9.3	53	
27	Ward No-08(part1)	CHTT	2.9	134	
28	Ward No-09 (Part1)	CHTT	7.0	78	

29	Ward No-13	CHTT	3.8	80	
30	Ward No-14	CHTT	1.4	75	
31	Ward No-15 (Part1)	CHTT	2.0	53	
32	Ward No-16	CHTT	2.4	53	
33	Ward No-20	CHTT	0.5	33	
34	Ward No-21	CHTT	0.9	40	
35	Ward No-22	CHTT	0.9	35	
36	Ward No-30 (Part)	CHTT	0.9	46	
37	Ward No-31	CHTT	0.9	18	
38	Ward No-32	CHTT	0.9	24	
39	Ward No-33	CHTT	0.6	27	
40	Ward No-34	CHTT	1.0	35	
41	Ward No-35 (part)	CHTT	0.3	31	
42	Ward No-09 (Part)	CHTT	0.6	78	
43	Ward No-10	CHTT	6.2	42	
44	Ward No-11 (Part)	CHTT	2.1	94	
45	Ward No-12 (Part)	CHTT	1.9	74	
46	Ward No-07	CHTT	3.7	126	
47	Ward No-08(part)	CHTT	3.3	134	
48	Ward No-15 (Part)	CHTT	0.4	52	
49	Ward No-39 (Part)	CHTT	5.8	106	54.48
50	Ward No-40	CHTT	13.6	89	53.42
51	Ward No-41	CHTT	18.1	44	29.65

N:B: CHTT is the short form of Chittagong City.